IOP PUBLISHING JOURNAL OF PHYSICS: CONDENSED MATTER

J. Phys.: Condens. Matter **22** (2010) 063102 (18pp) doi:10.1088/0953-8984/22/6/063102

TOPICAL REVIEW

Fundamental measure theory for hard-sphere mixtures: a review

Roland Roth

Max-Planck-Institut für Metallforschung, Heisenbergstraße 3, 70569 Stuttgart, Germany
and
ITAP, Universität Stuttgart, Pfaffenwaldring 57, 70569 Stuttgart, Germany

E-mail: Roland.Roth@mf.mpg.de

Received 4 December 2009, in final form 5 January 2010
Published 27 January 2010
Online at stacks.iop.org/JPhysCM/22/063102

Abstract

Hard-sphere systems are one of the fundamental model systems of statistical physics and represent an important reference system for molecular or colloidal systems with soft repulsive or attractive interactions in addition to hard-core repulsion at short distances. Density functional theory for classical systems, as one of the core theoretical approaches of statistical physics of fluids and solids, has to be able to treat such an important system successfully and accurately. Fundamental measure theory is up to date the most successful and most accurate density functional theory for hard-sphere *mixtures*. Since its introduction fundamental measure theory has been applied to many problems, tested against computer simulations, and further developed in many respects. The literature on fundamental measure theory is already large and is growing fast. This review aims to provide a starting point for readers new to fundamental measure theory and an overview of important developments.

Contents

1. Introduction

Density functional theory (DFT) for classical systems [1] is a versatile and powerful approach to study the equilibrium structure and corresponding thermodynamic quantities of many-body systems subjected to external potentials. Established in the 1970s, the basic formalism of classical DFT closely follows the quantum mechanical formulation [2–4]. There is a mathematical rigorous framework that proves the existence of a density functional of the grand potential $\Omega[\{\rho_i\}]$ and shows that for the equilibrium density profiles $\{\rho_i^0(\mathbf{r})\}$ it is minimal and equal to the grand potential $\Omega[\{\rho_i^0\}] = \Omega$ of the system. For applications the main problem is to construct a functional of the excess free energy, that contains all the information about the inter-particle interaction, for the system of interest. It turns out that a fluid of hard spheres, beside being of intrinsic interest, is an important reference system. At first, within the framework of classical DFT, mainly functionals for one-component systems were constructed. This changed in 1989.

In 1989, which was a remarkable year for classical DFT, Rosenfeld introduced his fundamental measure theory

(FMT) [5], which from the onset was a theory for hard-sphere *mixtures*. Also in 1989 Vanderlick *et al* [6] generalized Percus' *exact* one-dimensional DFT for hard rods [7] to mixtures. Rosenfeld's FMT and the exact one-dimensional functional share the same structure: both theories use weighted densities, which are convolutions of the local densities with geometrical weight functions, and in both theories the excess free energy density is a function of these weighted densities. Interestingly, Rosenfeld did not seem to be aware of the exact hard-rod mixture functional, as he never cited it in his work, but always referred to Percus' earlier one-component functional. Rosenfeld built FMT based on ideas from scaled-particle theory (SPT) [8] and the insight into the bulk behavior of hard-sphere mixtures from Percus–Yevick (PY) integral equation theory [9, 10]. Shortly before Rosenfeld published his hard-sphere functional, he arrived at a point of view in which SPT and PY started to converge [11].

Similar to Tarazona and Evans [12], who used the step-like Mayer-f function, that describes the interaction between two hard spheres as a weight function, Rosenfeld constructed FMT so that it makes use of the geometrical interpretation of Mayer clusters in hard-sphere systems. Rosenfeld, however, made use of the geometrical characteristics of individual particles rather than of a Mayer-f function of a two-sphere interaction. Although the interpretation of a Mayer cluster in terms of fundamental geometrical measures of the individual particles seems unnecessarily complicated, if only a one-component system is considered, it was the essential step for a mixture theory.

At first, when applied to hard-sphere fluids, FMT seemed to succeed in solving all problems. Kierlik and Rosinberg derived a FMT functional using different weight functions, based on an alternative deconvolution of the Mayer-f function [13]. Later it could be proven that both approaches are equivalent [14].

However, FMT failed to account for the freezing transition of the hard-sphere fluid into a solid. Rosenfeld *et al* analyzed the reason for this shortcoming. It became clear that the excess free energy density of a highly confined fluid diverged, which first was fixed empirically [15, 16] by modifying that part of the functional that caused the divergence. These ideas were based on the dimensional crossover, i.e. confining a three-dimensional fluid, described by a three-dimensional theory, to two, one or even to zero dimensions by suitable confining potentials. Later Tarazona and Rosenfeld fixed the problem more systematically. Tarazona introduced tensorial weighted densities [17] and thereby lifted the divergence of the original FMT. Now FMT could account for the freezing transition.

One drawback of Tarazona's tensorial FMT was that the underlying thermodynamics was still based on the PY equation of state, as is the case of Rosenfeld's original FMT. As a consequence the coexisting densities of the pure system between the hard-sphere fluid and the solid were clearly shifted [18–20] compared to the known simulation results [21, 22]. This could be solved by empirically modifying the underlying equation of state from the PY compressibility equation to the expression of Mansoori–Carnahan–Starling–Leland (MCSL) [23]. The resulting functional clearly improved the results for the coexisting densities [18, 19].

As hinted at in this short introduction, FMT not only succeeds in describing the properties of a hard-sphere fluid and solid, and thereby acting as a suitable reference system for systems with additional soft repulsive or attractive interactions, but it also gives insight into problems of statistical physics of excluded volume from a more fundamental point of view. Although the framework of FMT introduces some approximations, it is very appealing and powerful.

In this review I present the theory of FMT, some applications and some hints about the implementation of a FMT functional in simple geometries. In section 2 I recall a few properties of DFT and give the Mayer-cluster expansion of the excess free energy up to third order in the density. However, this section is not meant as an introduction to DFT. Those who are new to DFT should study [1] and [24] first. The first key idea of FMT is presented in section 3, where the deconvolution of the Mayer-f function into geometrical weight functions is presented. Based on the deconvolution, Rosenfeld made an ansatz for the excess free energy density. The extrapolation from the exact low density limit to higher densities can be performed in various ways, as discussed in section 4. Three schemes are discussed: Rosenfeld's derivation is presented first in section 4.1. Ideas based on the dimensional crossover follow in section 4.2. Finally, a derivation of FMT, based on a known, accurate equation of state for mixtures, is given in section 4.3. From a practical point of view, it seems natural to combine ideas from all approaches in order to construct the functional best suited for the given purpose, as indicated in section 4.4.

Some applications of FMT to the hard-sphere fluid, section 5, and to the hard-sphere solid, section 6, are presented to give the reader a flavor of the accuracy and reliability of FMT. Since its introduction FMT has stimulated the field of classical DFT in many respects. While this review is restricted to the theory of hard-sphere mixtures, some examples to developments of theories for other models with spherical particles, inspired by FMT, are given in section 7. This section is in no sense a complete review of recent developments. Some practical aspects of the implementation of FMT are touched upon in section 8, before I conclude in section 9.

With this outline, I hope to provide a good starting point for the reader new to FMT as well as a reference for those who are already experienced in applying FMT.

2. Density functional theory

In the framework of density functional theory [1, 24] it can be shown rigorously for a ν-component mixture in the grand ensemble that there exists a functional of the one-body density profiles $\{\rho_i\}$, $i = 1, \ldots, \nu$, of the form

$$\Omega[\{\rho_i\}] = \mathcal{F}[\{\rho_i\}] + \sum_{i=1}^{\nu} \int \mathrm{d}^3 r\, \rho_i(\mathbf{r}) \left(V_{\mathrm{ext}}^i(\mathbf{r}) - \mu_i\right), \quad (1)$$

with μ_i and $V_{\mathrm{ext}}^i(\mathbf{r})$ the chemical and the external potential of species i, respectively. This functional has two important properties: (i) for the equilibrium density profiles $\{\rho_i^0(\mathbf{r})\}$ the functional reduces to the grand potential of the system $\Omega[\{\rho_i^0\}] = \Omega$. (ii) for any other density profiles the functional

reduces to a value that is larger than the grand potential: $\Omega[\{\rho_i \neq \rho_i^0\}] > \Omega$. These two properties can be summarized by the variational principle

$$\left.\frac{\delta\Omega[\{\rho_i\}]}{\delta\rho_i(\mathbf{r})}\right|_{\{\rho_i(\mathbf{r})=\rho_i^0(\mathbf{r})\}} = 0.$$

The functional $\mathcal{F}[\{\rho_i\}]$ of the intrinsic Helmholtz free energy in equation (1) can be split into two parts:

$$\mathcal{F}[\{\rho_i\}] = \beta^{-1}\sum_{i=1}^{\nu}\int \mathrm{d}^3r\,\rho_i(\mathbf{r})(\ln\lambda_i^3\rho_i(\mathbf{r}) - 1) + \mathcal{F}_{\mathrm{ex}}[\{\rho_i\}],$$

with $\beta = 1/(k_\mathrm{B}T)$, where k_B is the Boltzmann constant and T the temperature. The first term is the exactly known ideal gas contribution to the intrinsic free energy and all the information about interactions between particles is in the second term, the excess (over the ideal gas) free energy. In contrast to the ideal gas contribution, the excess free energy functional $\mathcal{F}_{\mathrm{ex}}[\{\rho_i\}]$ is not known exactly, but for particles interacting via pair interactions $V_{ij}(r)$ an expansion at low densities can be given:

$$\begin{aligned}\beta\mathcal{F}_{\mathrm{ex}}[\{\rho_i\}] = &-\tfrac{1}{2}\sum_{i,j}\int \mathrm{d}^3r_1\int \mathrm{d}^3r_2\,\rho_i(\mathbf{r}_1)\rho_j(\mathbf{r}_2)f_{ij}(r_{12})\\ &-\tfrac{1}{6}\sum_{i,j,k}\int \mathrm{d}^3r_1\int \mathrm{d}^3r_2\int \mathrm{d}^3r_3\,\rho_i(\mathbf{r}_1)\rho_j(\mathbf{r}_2)\rho_k(\mathbf{r}_3)\\ &\times f_{ij}(r_{12})f_{ik}(r_{13})f_{jk}(r_{23}) + \mathcal{O}(\rho^4)\end{aligned} \tag{2}$$

with $r_{ij} = |\mathbf{r}_i - \mathbf{r}_j|$ and the Mayer-f function defined by

$$f_{ij}(r) = \exp(-\beta V_{ij}(r)) - 1.$$

In the case of hard-sphere interactions $f_{ij}(r)$ has a purely geometrical interpretation:

$$V_{ij}(r) = \begin{cases}\infty & r < R_i + R_j\\ 0 & \text{otherwise,}\end{cases}$$

$$\Rightarrow f_{ij}(r) = \begin{cases}-1 & r < R_i + R_j\\ 0 & \text{otherwise,}\end{cases}$$

i.e. the Mayer-f function marks the volume that is not accessible to the center of one sphere, say of species i, close to another sphere of species j. This excluded volume is the volume of a sphere of radius $R_i + R_j$.

3. Deconvolution

Interestingly, V_{i+j}, the volume of two joined convex bodies i and j, can in general be written as [25]

$$V_{i+j} = V_i + S_iR_j + R_iS_j + V_j, \tag{3}$$

where V_k, S_k, and R_k are the volume, the surface area and the mean radius of curvature of the body $k = i, j$, respectively. The volume of the joined body can be expressed in terms of geometrical measures of the individual bodies. In odd dimensions this integral relation between geometrical measures can also be expressed locally, which leads to the deconvolution of the Mayer-f function.

Rosenfeld noted that the Mayer-f function for hard-sphere mixtures in $3d$ can be decomposed into [5]

$$\begin{aligned}-f_{ij}(r) = &\,\omega_3^i\otimes\omega_0^j + \omega_0^i\otimes\omega_3^j + \omega_2^i\otimes\omega_1^j\\ &+ \omega_1^i\otimes\omega_2^j - \vec{\omega}_2^i\otimes\vec{\omega}_1^j - \vec{\omega}_1^i\otimes\vec{\omega}_2^j\end{aligned} \tag{4}$$

with the weight functions given by

$$\omega_3^i(\mathbf{r}) = \Theta(R_i - r),$$

$$\omega_2^i(\mathbf{r}) = \delta(R_i - r),$$

$$\vec{\omega}_2^i(\mathbf{r}) = \frac{\mathbf{r}}{r}\delta(R_i - r),$$

and $\omega_1^i(\mathbf{r}) = \omega_2^i(\mathbf{r})/(4\pi R_i)$, $\omega_0^i(\mathbf{r}) = \omega_2^i(\mathbf{r})/(4\pi R_i^2)$, and $\vec{\omega}_1^i(\mathbf{r}) = \vec{\omega}_2^i(\mathbf{r})/(4\pi R_i)$. Here $\Theta(r)$ is the Heaviside step function and $\delta(r)$ is the Dirac-delta distribution. The symbol $\otimes$ in equation (4) denotes the three-dimensional convolution of the weight functions

$$\omega_i^\alpha\otimes\omega_j^\beta(\mathbf{r} = \mathbf{r}_i - \mathbf{r}_j) = \int \mathrm{d}\mathbf{r}'\,\omega_i^\alpha(\mathbf{r}' - \mathbf{r}_i)\omega_j^\beta(\mathbf{r}' - \mathbf{r}_j).$$

The deconvolution can be easily checked in Fourier space.

The connection between the deconvolution of the Mayer-f function in equations (4) and (3) becomes apparent when the weight functions are integrated. Integration over $\omega_\alpha^i(\mathbf{r})$ gives the volume V_i ($\alpha = 3$), the surface area S_i ($\alpha = 2$), the mean radius of curvature R_i ($\alpha = 1$) and the Euler characteristics, which is simply 1 ($\alpha = 0$), which are the *fundamental* geometrical *measures* of a sphere of species i in $3d$. It is this property of FMT that gives the approach its name. The integrals over the vector-like weight functions vanish.

The deconvolution of the Mayer-f function derived by Rosenfeld is not unique. Kierlik and Rosinberg found an alternative that avoids the vector-like weight functions [13]:

$$-f_{ij}(r) = \omega_3^i\otimes\tilde{\omega}_0^j + \tilde{\omega}_0^i\otimes\omega_3^j + \omega_2^i\otimes\tilde{\omega}_1^j + \tilde{\omega}_1^i\otimes\omega_2^j, \tag{5}$$

where ω_3^i and ω_2^i are the same weight function that Rosenfeld found but the remaining weight functions are somewhat more complex than the Rosenfeld weights due to the presence of derivatives of the Dirac-delta distribution. They are given by [13]

$$\tilde{\omega}_1^i(\mathbf{r}) = \frac{1}{8\pi}\delta'(R_i - r),$$

$$\tilde{\omega}_0^i(\mathbf{r}) = -\frac{1}{8\pi}\delta''(R_i - r) + \frac{1}{2\pi r}\delta'(R_i - r).$$

While I will stick here to Rosenfeld's weight functions, there are two important points to make: (i) it was shown [14] that the approaches based on Rosenfeld's deconvolution, equation (4), and on Kierlik and Rosinberg's one, equation (5), are equivalent. This in turn implies that (ii) by comparing equation (4) with equation (5), it is possible to establish connections between terms containing the vector-like weight functions and corresponding scalar terms. This point will become of great importance in section 4, when the functional is derived by extrapolating from the exact low density limit to high densities.

The weight functions give rise to a set of weighted densities $\{n_\alpha(\mathbf{r})\}$ for the ν-component mixture. These are defined as [5, 26]

$$n_\alpha(\mathbf{r}) = \sum_{i=1}^{\nu} \int \mathrm{d}^3 r'\, \rho_i(\mathbf{r}')\omega_\alpha^i(\mathbf{r}-\mathbf{r}'), \tag{6}$$

i.e. as the sum of the convolutions of the density profiles of each species with its weight function. The exact one-dimensional functional for hard-rod mixtures possesses weight functions of this form [6]. Technically, the use of weight functions makes FMT a functional of the weighted density approximation (WDA) class. In the case of Rosenfeld's weight functions α labels four scalar and two vector weights. In the bulk, where the density profiles in the absence of any external field reduce to constant bulk densities ρ^i_{bulk}, both vector weighted densities $\vec{n}_1$ and $\vec{n}_2$ vanish while the scalar weighted densities reduce to the so-called SPT variables [8]: $n_3 \to \xi_3 = \sum_i \rho^i_{\mathrm{bulk}} 4\pi R_i^3/3$, the total packing fraction, $n_2 \to \xi_2 = \sum_i \rho^i_{\mathrm{bulk}} 4\pi R_i^2$, $n_1 \to \xi_1 = \sum_i \rho^i_{\mathrm{bulk}} R_i$ and $n_0 \to \xi_0 = \sum_i \rho^i_{\mathrm{bulk}}$.

The weighted densities, equation (6), are constructed so that the low density of the excess free energy, the first line of equation (2), can be recovered exactly:

$$\begin{aligned}\lim_{\{\rho_i\to 0\}} \beta\mathcal{F}_{\mathrm{ex}}[\{\rho_i\}] &= -\tfrac{1}{2}\sum_{i,j}\int \mathrm{d}^3 r_1 \int \mathrm{d}^3 r_2\, \rho_i(\mathbf{r}_1) \\ &\quad\times \rho_j(\mathbf{r}_2) f_{ij}(r_{12}) \\ &= \int \mathrm{d}^3 r\, \{n_0(\mathbf{r})n_3(\mathbf{r}) + n_1(\mathbf{r})n_2(\mathbf{r}) - \vec{n}_1(\mathbf{r})\cdot\vec{n}_2(\mathbf{r})\}. \end{aligned}\tag{7}$$

The next order term, the second and third lines of equation (2), however cannot be reproduced exactly with the weight functions obtained from the deconvolution of the Mayer-f function, because the structure of the integrals are not simple convolutions. In fact, it can be shown that in order to calculate the volume of a set of $N \geqslant 4$ overlapping spheres in $d = 3$, it is in general necessary to consider two-, three-, and four-sphere overlaps [27].

4. Extrapolation to higher densities

Rosenfeld suggested for the excess free energy functional the form

$$\beta\mathcal{F}_{\mathrm{ex}}[\{\rho_i\}] = \int \mathrm{d}^3 r'\, \Phi(\{n_\alpha(\mathbf{r}')\}) \tag{8}$$

where Φ, the reduced free energy density, is a *function* of the weighted densities and not a functional. This form follows that of the exact one-dimensional functional [7, 6] and recovers the exact low density limit, equation (7).

As ansatz for Φ Rosenfeld, employed dimensional analysis and used [5]

$$\begin{aligned}\Phi &= f_1(n_3)n_0 + f_2(n_3)n_1n_2 + f_3(n_3)\vec{n}_1\cdot\vec{n}_2 \\ &\quad + f_4(n_3)n_2^3 + f_5(n_3)n_2\vec{n}_2\cdot\vec{n}_2. \end{aligned}\tag{9}$$

Each term in (9) has the dimension of a number density, i.e. [length] $^{-3}$. In order to ensure that the ansatz, equations (8) and (9), recovers the deconvolution of the Mayer-f function, equation (4), and the pair direct correlation function up to first order in density, it is necessary to demand that the unknown functions $f_1, \ldots, f_5$ have low density expansions of the form $f_1 = n_3 + n_3^2/2 + \mathcal{O}(n_3^3)$, $f_2 = 1 + n_3 + \mathcal{O}(n_3^2)$, $f_3 = -1 - n_3 + \mathcal{O}(n_3^2)$, $f_4 = 1/24\pi + \mathcal{O}(n_3)$, and $f_5 = -3/24\pi + \mathcal{O}(n_3)$. It is possible to go one step further. Since the deconvolution of the Mayer-f function due to Rosenfeld [5] and that due to Kierlik and Rosinberg [13] are equivalent, one can conclude that connections between the functions f_2 and f_3, and between f_4 and f_5 should hold for arbitrary densities, not only in the low density limit. In general, these conditions are

$$f_3(n_3) = -f_2(n_3) \tag{10}$$

$$f_5(n_3) = -3f_4(n_3), \tag{11}$$

so that the ansatz, equation (9), simplifies to

$$\Phi = f_1(n_3)n_0 + f_2(n_3)(n_1n_2 - \vec{n}_1\cdot\vec{n}_2) + f_4(n_3)(n_2^3 - 3n_2\vec{n}_2\cdot\vec{n}_2). \tag{12}$$

These equations are rather important because they justify the use of thermodynamic relations, for which the vector weighted densities vanish, to extrapolate the excess free energy density from the known low density limit to higher densities.

The actual extrapolation to higher densities can be performed in various ways. Rosenfeld used a differential equation from scaled-particle theory. His derivation of FMT is presented in section 4.1. The resulting functional, however, failed to predict a freezing transition of the hard-sphere fluid into a solid. A careful analysis showed that the functional diverged in highly confined situations. This insight gave rise to the dimensional crossover, in which the three-dimensional functional was employed to study two-, one-, and zero-dimensional density distributions. The dimensional crossover was also used to construct a functional with new tensorial weighted densities, which successfully could describe the freezing transition, as discussed in section 4.2. A third way of extrapolation uses a known equation of state as input and leads to the White-Bear version of FMT, reviewed in section 4.3. Yet another way, which will be mentioned here, but not discussed, follows Percus [26], and starts from the knowledge of a bulk pair direct correlation function to construct the excess free energy functional [28].

4.1. Rosenfeld's derivation

The functions $f_1, \ldots, f_5$, or f_1, f_2 and f_4 together with conditions (10) and (11), can be determined by demanding that the resulting functional satisfies a thermodynamic condition. In the original derivation Rosenfeld used the SPT equation [8]

$$\lim_{R_i\to\infty} \frac{\beta\mu^i_{\mathrm{ex}}}{V_i} = \beta p, \tag{13}$$

with $V_i = 4\pi R_i^3/3$, the volume of a spherical particle with radius R_i, and μ^i_{ex} the excess chemical potential of species i. This equation relates the excess chemical potential for the insertion of a big sphere with radius R_i into a hard-sphere fluid to the leading order term pV_i of the reversible work necessary to create a cavity big enough to hold this particle. The l.h.s.

of equation (13) can be determined in terms of the weighted densities from equation (8)

$$\beta\mu_{\rm ex}^{i} = \frac{\partial\Phi}{\partial\rho_i} = \sum_{\alpha}\frac{\partial\Phi}{\partial n_\alpha}\frac{\partial n_\alpha}{\partial\rho_i}.$$

Due to the geometrical meaning of the weight functions, one finds $\partial n_3/\partial\rho_i = 4\pi/3R_i^3 \equiv V_i$, $\partial n_2/\partial\rho_i = 4\pi R_i^2 \equiv S_i$, $\partial n_1/\partial\rho_i = R_i$, and $\partial n_0/\partial\rho_i = 1$. In the limit $R_i \to \infty$, all but the first term vanish and one obtains

$$\lim_{R_i\to\infty}\frac{\beta\mu_{\rm ex}^{i}}{V_i} = \frac{\partial\Phi}{\partial n_3} = \beta p. \tag{14}$$

The equation of state can be obtained from the thermodynamic bulk relation $\Omega_{\rm bulk} = -pV$. Since the grand potential density in the bulk is $\Omega_{\rm bulk}/V = \Phi + f_{id} - \sum_i \rho_{\rm bulk}^{i}\mu_i$ one obtains

$$\beta p = -\Phi + \sum_{\alpha}\frac{\partial\Phi}{\partial n_\alpha}n_\alpha + n_0. \tag{15}$$

The last term in equation (15), n_0, results from the ideal gas contribution. Combining these results leads to the SPT differential equation

$$\frac{\partial\Phi}{\partial n_3} = -\Phi + \sum_{\alpha}\frac{\partial\Phi}{\partial n_\alpha}n_\alpha + n_0.$$

By collecting all terms proportional to n_0 one sees that the differential equation for $f_1(n_3)$ takes the form

$$f_1'(n_3)(1-n_3) = 1,$$

where $'$ indicates a derivative w.r.t. n_3. This equation is solved by

$$f_1(n_3) = {\rm const}_1 - \ln(1-n_3),$$

with an integration constant $\rm const_1$ that vanishes, in order to recover the low density limit. It is easy to identify and solve the differential equations for the remaining functions

$$f_2'(n_3)(1-n_3) = f_2(n_3) \Rightarrow f_2(n_3) = \frac{{\rm const}_2}{1-n_3}$$

and

$$f_4'(n_3)(1-n_3) = 2f_4(n_3) \Rightarrow f_4(n_3) = \frac{{\rm const}_3}{(1-n_3)^2}.$$

The integration constants are chosen so that the correct behavior at low densities is recovered. The solution found by Rosenfeld [5], denoted by RF, is

$$f_1^{\rm RF}(n_3) = -\ln(1-n_3)$$

$$f_2^{\rm RF}(n_3) = \frac{1}{1-n_3}$$

$$f_4^{\rm RF}(n_3) = \frac{1}{24\pi(1-n_3)^2}$$

and it is straightforward to see that these solutions recover the low density limit. The full excess free energy density then is

$$\Phi^{\rm RF} = -n_0\ln(1-n_3) + \frac{n_1n_2 - \vec{n}_1\cdot\vec{n}_2}{1-n_3} + \frac{n_2^3 - 3n_2\vec{n}_2\cdot\vec{n}_2}{24\pi(1-n_3)^2}. \tag{16}$$

It is remarkable that the Rosenfeld functional generates as output the mixture Percus–Yevick compressibility equation of state and the PY direct correlation functions $c_{ij}^{(2)}(r)$ [5].

While the original Rosenfeld functional, as described in this subsection, turns out to accurately describe the structure and thermodynamics of the fluid phase of hard-sphere mixtures [29], it failed to account for the hard-sphere crystal [5]. One possible interpretation of a crystal is that each particle on a lattice is confined to a small cavity, created by the neighbor particles, that can hold only a single particle. Hence, in order to describe a crystal, a functional has to be able to cope with strong confinement.

4.2. Dimensional crossover

The idea of dimensional crossover is simple, yet very powerful. The hypothetical *exact* functional for hard spheres in three dimension would reduce to the hypothetical exact functional in two dimensions, if the density distribution inputted into the three-dimensional functional was restricted to a plane, i.e. $\rho_i(\mathbf{r}) = \delta(z)\rho_i(x,y)$. Furthermore, the hypothetical exact functional for hard spheres in three dimensions would recover the exact one-dimensional functional if the density distribution inputted into the three-dimensional functional was restricted to a line, i.e. $\rho_i(\mathbf{r}) = \delta(z)\delta(y)\rho_i(x)$.

Kierlik and Rosinberg [30] asked for the FMT functional a slightly simpler question, thereby following Tarazona *et al* [31], who first applied the idea of dimensional crossover for a different WDA functional. The idea was quickly picked up by Rosenfeld [32]. Kierlik and Rosinberg considered the two-dimensional limit by using a three-dimensional density distribution of the form $\rho_i(\mathbf{r}) = \delta(z)\rho_i^{(2D)}$, with homogeneous two-dimensional bulk densities $\rho_i^{(2D)}$. The resulting excess free energy density was then compared with accurate, known results. Note that the homogeneous two-dimensional system is described as an inhomogeneous, highly confined three-dimensional system. Hence, the weighted densities, equation (6), which can be calculated straightforwardly, depend on z [16]. The resulting excess free energy can be obtained from equation (8) through integration of the excess free energy density. The resulting excess free energy per particle differs in functional form significantly from the rather accurate SPT expression but numerically agrees with it rather nicely [30, 32]. As a side note I mention that the two-dimensional limit of the White-Bear version of FMT, described in section 4.3, results in an even more complex functional form of the excess free energy density, which numerically is even closer to the SPT result.

The one-dimensional limit of the three-dimensional FMT functional can be taken by considering density distributions of the form $\rho_i(\mathbf{r}) = \delta(x)\delta(z)\rho_i^{(1D)}$. Analogous to the two-dimensional limit, it is straightforward to calculate the three-dimensional weighted densities [16]. However, the integral of the excess free energy density, equation (8), does not exist. The integration of the first two terms of equation (16) recovers the *exact* one-dimensional excess free energy, while the third term diverges [30, 32].

A first step in resolving this severe problem was to consider also the zero-dimensional limit, in which a small

cavity is studied that can hold only a single sphere. The thermodynamics of such a small cavity is known exactly and it was found numerically that the exact zero-dimensional limit for a spherical cavity can be recovered if the last term of equation (16) is replaced by [16]

$$\Phi_3^{0D} = \frac{3n_2^3\xi(1-\xi)^2}{24\pi(1-n_3)^2}, \tag{17}$$

with $\xi(\mathbf{r}) = |\vec{n}_2(\mathbf{r})/n_2(\mathbf{r})|$. While the divergence in the one-dimensional limit is removed and the exact zero-dimensional limit is recovered, this empirical modification of FMT has the unfortunate side-effect of changing the bulk properties of the three-dimensional fluid. In the bulk limit $\xi \to 0$, so that equation (17) vanishes [16]. Still, the study of the zero-dimensional limit provided the insight that the divergence of the third term of equation (16) can be resolved by *anti-symmetrizing* it. As alternative to equation (17), Rosenfeld *et al* suggested [15, 16]

$$\Phi_3^{\text{asym}-q} = \frac{n_2^3(1-\xi)^q}{24\pi(1-n_3)^2}, \tag{18}$$

with $q \geqslant 2$. The anti-symmetrized expression with $q = 3$ makes only small errors in the zero-dimensional limit and describes the three-dimensional fluid accurately, because the deviation from the original expression in equation (16) is of the order of ξ^4 [15, 16]. This empirical modification of the Rosenfeld functional allowed the first studies of hard-sphere crystals with FMT [16].

One interesting property of the zero-dimensional limit is that its free energy does not depend on the shape of the cavity, i.e. the confining potential, but on the fact that the cavity can hold only a single particle. While equation (18) works for spherical cavities, it still would diverge for small cavities of peculiar shape that can hold only a single particle [33].

A FMT functional, built on the idea to recover the exact zero-dimensional limit even for some peculiar shaped cavities, the so-called *lost cases*, was suggested by Tarazona and Rosenfeld [33, 34]. This idea results in a functional for the one-component hard-sphere system that shares the first two terms with the original Rosenfeld functional, equation (16), but modifies the third term. The third term is constructed so that it vanishes in the one-dimensional limit [33]. Unfortunately, this functional, similar to the results of the empirical approach in [15, 16], cannot recover important bulk properties of the hard-sphere fluid. While the equation of state of the functional is the PY compressibility equation, the direct correlation function differs severely from the PY result [17].

Tarazona resolved this problem by introducing an additional tensorial weight function [17], which in the notation of [35], is given by

$$\omega^i_{m_2}(\mathbf{r}) = \left(\frac{1}{r^2}\mathbf{rr} - \frac{1}{3}\hat{1}\right)\omega_2^i(\mathbf{r}), \tag{19}$$

which gives rise to a tensorial weighted density n_{m_2}. $\hat{1}$ denotes the unit matrix. The modified third term of the Tarazona FMT, Φ_3^{T}, makes use of the unique combination of the scalar, vectorial, and tensorial weighted densities n_2, $\vec{n}_2$, and n_{m_2}, respectively, that in the bulk limit recovers the PY pair direct correlation function [36]. It is given by [17, 35]

$$\Phi_3^{\text{T}} = \{n_2^3 - 3n_2\vec{n}_2\cdot\vec{n}_2 + 9(\vec{n}_2 n_{m_2}\vec{n}_2 - \tfrac{1}{2}\text{Tr}(n_{m_2}^3))\} \times \frac{1}{24\pi(1-n_3)^2}. \tag{20}$$

This version of FMT with a tensorial weighted density systematically corrects the problem of the diverging excess free energy for highly confined particles and allows for a successful description of the hard-sphere solid [17].

Interestingly, the tensorial weighted density in its original form [17] also appears in a FMT functional for non-spherical hard particles [37], which systematically improves Rosenfeld's functional for convex hard bodies [38, 39]. The dimensional crossover was analyzed numerically by Gonzalez *et al* [40].

4.3. The White-Bear version of FMT

In contrast to the original Rosenfeld derivation, it is possible to use a mixture equation of state, if it can be written solely in terms of the SPT variables, as an *input* to the extrapolation from the low density limit to higher densities. To this end the *known* equation of state is combined with equation (15), the expression for the pressure within FMT. This approach employs as starting point, of course, the same weight functions and weighted densities, and the same ansatz as the Rosenfeld functional.

An obvious choice for the mixture equation of state is the Mansoori–Carnahan–Starling–Leland (MCSL) equation of state [23], which is a generalization to the ν-component hard-sphere fluid of the accurate, one-component Carnahan–Starling–Boublík equation of state p_{CS} [41, 42], given by

$$\beta p_{\text{MCSL}} = \frac{n_0}{1-n_3} + \frac{n_1 n_2}{(1-n_3)^2} + \frac{n_2^3}{12\pi(1-n_3)^3} - \frac{n_3 n_2^3}{36\pi(1-n_3)^3}. \tag{21}$$

Note that the final term in (21) is absent in the PY compressibility equation of state. Compared to computer simulation data the MCSL pressure is significantly more accurate than the PY result [43].

The differential equation for determining the three unknown functions f_1, f_2, and f_4 of ansatz (12) follow from

$$\beta p_{\text{input}} = -\Phi + \sum_\alpha \frac{\partial\Phi}{\partial n_\alpha} n_\alpha + n_0, \tag{22}$$

with the sum over the scalar weighted densities only. Again, one obtains differential equations for f_1, f_2 and f_4 by collecting all the terms proportional to n_0, $n_1 n_2$, and n_2^3, respectively. For $p_{\text{input}} = p_{\text{MCSL}}$ these differential equations can be solved easily and one finds $f_1(n_3) = f_1^{\text{RF}}(n_3)$, $f_2(n_3) = f_2^{\text{RF}}(n_3)$ and

$$f_4(n_3) = \frac{n_3 + (1-n_3)^2\ln(1-n_3)}{36\pi n_3^2(1-n_3)^2}.$$

The excess free energy density is obtained by combining f_1, f_2, and f_4 with equations (10) and (11) to give [19]

$$\Phi^{\mathrm{WB}} = -n_0 \ln(1-n_3) + \frac{n_1 n_2 - \vec{n}_1 \cdot \vec{n}_2}{1-n_3} + (n_2^3 - 3n_2 \vec{n}_2 \cdot \vec{n}_2) \frac{n_3 + (1-n_3)^2 \ln(1-n_3)}{36\pi n_3^2 (1-n_3)^2}, \quad (23)$$

which should be compared with the original Rosenfeld form, equation (16). This functional was named after the institution in Bristol in which it was derived, as mentioned in the acknowledgments of [19].

Like the Rosenfeld functional this functional, the White-Bear version of FMT, recovers the exact low density limit. Interestingly, this excess free energy density was first mentioned in 1990 as a side note by Kierlik and Rosinberg [13] using their weight functions. Only much later was it put to use. Tarazona used a one-component version, using his own notation, to study the hard-sphere solid [18]. Lang [20] employed the White-Bear version of FMT [19] before publication during his PhD work. Slightly later the White-Bear version of FMT was also published by Yu *et al* [44].

The SPT differential equation (14), which is of central importance to the derivation of the original Rosenfeld functional, obviously cannot be satisfied by the White-Bear version of FMT. Since equation (14) is an exact thermodynamic relation, this is a shortcoming of FMT. With the weight functions of FMT the only non-trivial equation of state that satisfies equation (14) is the PY compressibility result. Any equation of state that is more accurate than PY, and which can be written in terms of the SPT variables, must lead to an inconsistency in equation (14). For the White-Bear version of FMT, one finds from equation (23) in the bulk limit that [19]

$$\frac{\partial \Phi}{\partial n_3} = \frac{n_0}{1-n_3} + \frac{n_1 n_2}{(1-n_3)^2} - \frac{n_2^3 (2 + n_3(n_3-5))}{36\pi n_3^2 (1-n_3)^3} - \frac{n_2^3 \ln(1-n_3)}{18\pi n_3^3}, \quad (24)$$

which evidently is different from the MCSL equation of state (21). The difference arising from this inconsistency was examined within the context of the one-component fluid [19]. The deviation between p_{CS} and equation (24) in the fluid regime is at most 2%. In contrast, the Percus–Yevick compressibility equation of state p^c_{PY} overestimates the pressure of a hard-sphere fluid close to freezing by up to 7%.

Based on the observation that the MCSL equation of state leads to an excess free energy density that is slightly inconsistent, recently a new generalization of the Carnahan–Starling–Boublík equation of state to mixtures was proposed [45]. The idea of this equation of state is simple. Consider the following loop: start with an equation of state, expressed in the SPT variables that reduce to p_{CS}, the Carnahan–Starling–Boublík pressure [41, 42], in the one-component case and integrate it to obtain the excess free energy density Φ. Within FMT the derivative of Φ w.r.t. n_3 should be again the equation of state, i.e. equation (14). Only with the PY compressibility equation of state is it possible to run this loop consistently for a mixture. The new equation of state minimizes the inconsistency obtained in this loop. It is given by [45]

$$\beta p_{\mathrm{CSIII}} = \frac{n_0}{1-n_3} + \frac{n_1 n_2 \left(1 + \frac{1}{3} n_3^2\right)}{(1-n_3)^2} + \frac{n_2^3 \left(1 - \frac{2}{3} n_3 + \frac{1}{3} n_3^2\right)}{12\pi (1-n_3)^3}. \quad (25)$$

This equation of state is found to represent data for binary and ternary mixtures obtained by computer simulations more accurate than the MCSL result [45]. Based on this new equation of state, using equation (22) with $p_{\mathrm{input}} = p_{\mathrm{CSIII}}$ an excess free energy functional can be derived, which improves the level of self-consistency [46]:

$$\Phi^{\mathrm{WBII}} = -n_0 \ln(1-n_3) + (n_1 n_2 - \vec{n}_1 \cdot \vec{n}_2) \frac{1 + \frac{1}{3}\phi_2(n_3)}{1-n_3} + (n_2^3 - 3n_2 \vec{n}_2 \cdot \vec{n}_2) \frac{1 - \frac{1}{3}\phi_3(n_3)}{24\pi (1-n_3)^2}$$

with

$$\phi_2(n_3) = \frac{1}{n_3}(2n_3 - n_3^2 + 2(1-n_3)\ln(1-n_3)),$$

and

$$\phi_3(n_3) = \frac{1}{n_3^2}(2n_3 - 3n_3^2 + 2n_3^3 + 2(1-n_3)^2 \ln(1-n_3)).$$

This functional, the White-Bear version of FMT mark II, is similar in complexity as the White-Bear version, equation (23), or the Rosenfeld functional, equation (16), but is constructed such that for a one-component bulk fluid it reduces to the Carnahan–Starling–Boublík equation of state:

$$\frac{\partial \Phi}{\partial n_3} = \beta p_{\mathrm{CS}}.$$

4.4. FMT toolbox

Within the framework of FMT there are different approaches for extrapolating from low to high densities, as has been discussed in this section. Some ideas seem to be more systematic or more esthetic than others. However, it is important to keep in mind that one of the most important goals of FMT is to provide an accurate and versatile *numerical* tool to describe the structure and corresponding thermodynamic quantities of inhomogeneous hard-sphere mixtures. Rosenfeld's original FMT [5] is based on a few surprisingly simple, yet powerful, principles. The resulting functional allows one to study the fluid phase, but fails to account for the freezing transition. Functionals constructed so that the zero-dimensional limit, in which a particle is confined in a small cavity, is *fully* respected, like the functional based on equation (17) of that of [33], enable FMT to describe freezing, but at the same time some bulk properties of the hard-sphere fluid get spoiled. Some additional changes are required to fix these shortcomings: equation (17) is replaced by equation (18) or a tensorial weight function, equation (19), is added to the set of FMT weight functions [17] in order to improve the functional of [33].

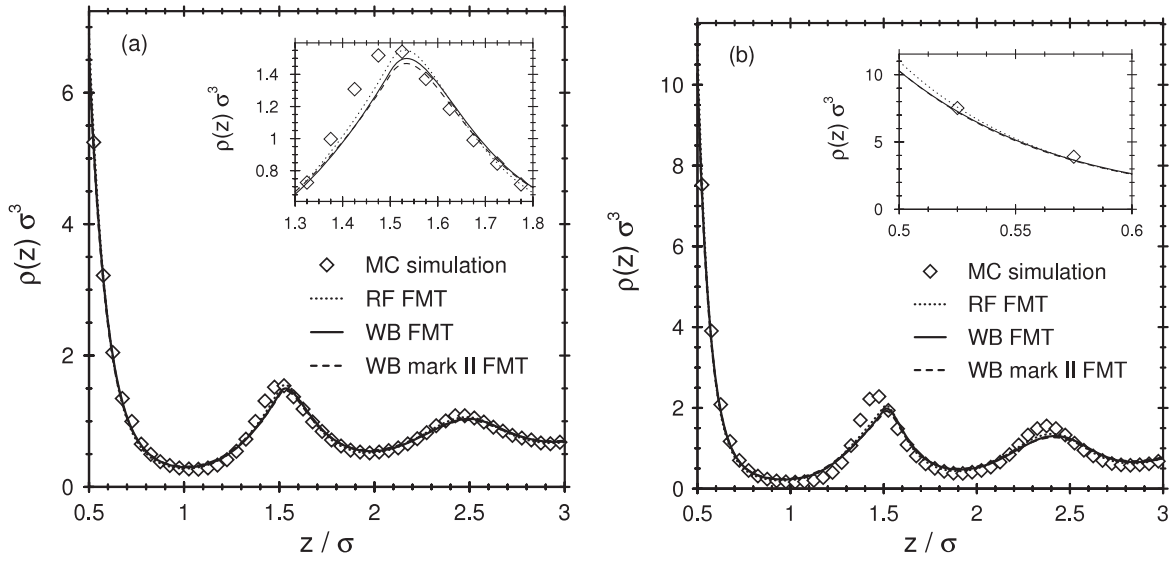

Figure 1. The density profiles of a pure hard-sphere fluid at a planar hard wall with bulk packing fraction of (a) $\eta = 0.4257$ and (b) $\eta = 0.4783$. Contact with the wall is at $z = \sigma/2$. The original Rosenfeld version (dotted line), the White-Bear version (full line) and the White-Bear version mark II (dashed line) are compared to data from MC simulations (symbols) [48]. The agreement among the various versions of FMT is good and the simulation data are very well described for low and moderate packing fractions. At high packing fractions, see (b), the overall agreement between FMT and simulations is still good, but, especially for the first peak at $z \approx 1.5\sigma$, clear deviations between FMT and simulations exist.

From a practical point of view FMT provides a toolbox made from a few building blocks that could be combined depending on the objective of the numerical calculation. On the one hand FMT has the functions $f_1(n_3), \ldots, f_5(n_3)$ that only depend on the local packing fraction n_3. These building blocks determine to a large degree the underlying equation of state, i.e. PY, MCSL or equation (25). On the other hand there are functions of the other weighted densities, $n_0, \ldots n_2, \vec{n}_1, \vec{n}_2$, and possibly n_{m_2}, which ensure that the bulk direct correlation functions and the behavior of the fluid under strong confinement are sensible.

As the derivation of the White-Bear version of FMT started from the same ansatz as Rosenfeld did, it obviously faces problems when applied to the freezing transition. However, it is possible to apply the empirical modification of [15, 16], as was done in [47], or the systematic change due to Tarazona [17], as was done in [19]. For example, by replacing the term $(n_2^3 - 3n_2\vec{n}_2 \cdot \vec{n}_2)$ in equation (23) by the numerator of Tarazona's expression, equation (20), the third term of the *White-Bear-tensor* functional would be given by [19, 18, 20]

$$\Phi_3^{\mathrm{WB,T}} = \{n_2^3 - 3n_2\vec{n}_2 \cdot \vec{n}_2 + 9(\vec{n}_2 n_{m_2}\vec{n}_2 - \tfrac{1}{2}\,\mathrm{Tr}(n_{m_2}^3))\} \times \frac{n_3 + (1-n_3)^2 \ln(1-n_3)}{36\pi n_3^2 (1-n_3)^2}.$$

Of course other combinations of the different *building blocks* are possible, if required by the application.

5. Properties of the fluid phase

DFT allows one to study the inhomogeneous structure of a fluid subjected to an external potential and corresponding thermodynamic quantities within the same framework. Before applying a functional to a complicated problem, its performance in simple, well understood situations should be established. In order to verify the accuracy of a particular functional it is helpful to compare DFT results to data from other approaches, such as computer simulations. Often this is done solely for density profiles. However, it is important to also verify the accuracy of thermodynamic quantities, such as the wall surface tension.

A standard problem for FMT is the prediction of the structure and wall surface tension of a hard-sphere fluid close to a planar hard wall. It is known that the density at the wall, the so-called contact density, equals the bulk pressure of the system divided by $k_{\mathrm{B}}T$. Since FMT is a WDA functional, the contact theorem, as discussed below, is satisfied. Therefore it is possible to conclude that close to the wall a version of FMT that is based on the Carnahan–Starling–Boublík equation of state [41, 42] should be more accurate compared to those based on the Percus–Yevick pressure. While for low and intermediate bulk packing fractions the difference between these two equations of state is rather small, it becomes more important close to the bulk freezing density.

In figure 1 two density profiles of a pure hard-sphere fluid at bulk packing fraction $\eta = 0.4257$ (a) and $\eta = 0.4783$ (b), as obtained from the original Rosenfeld functional (dotted line), from the White-Bear version of FMT (full line) and from the White-Bear version of FMT mark II (dashed line), are compared to data from Monte Carlo (MC) simulations [48] (symbols). Overall, the agreement between the various versions of FMT and the MC data is very good. One has to look closely to see differences among these results. For $\eta = 0.4257$, the density around the first peak is highlighted in the inset of figure 1(a). There are small deviations between FMT and the simulation data, and it seems as if the original

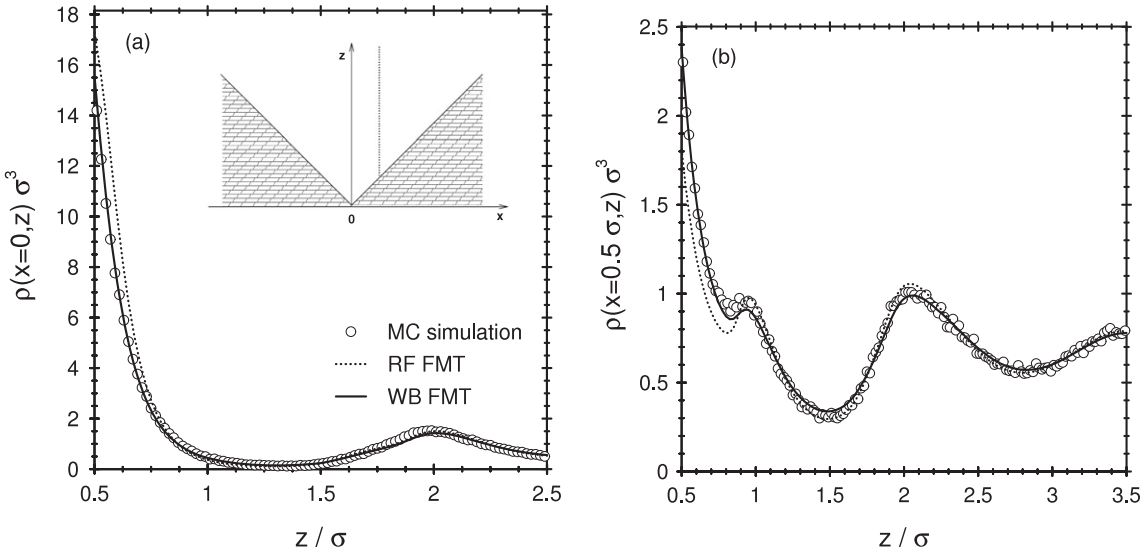

Figure 2. Cut through the density profile $\rho(x, z)$ of a hard-sphere fluid with $\eta = 0.3665$ in a hard wedge with opening angle of 90° from the Rosenfeld FMT (dotted line), the White-Bear version of FMT (full line) and MC simulations (symbols) [47]. The coordinates x and z are defined as indicated in the inset of (a), where z is relative to the surface and $z = \sigma/2$ denotes contact. In the middle of the wedge, $x = 0$, the contact density is extremely high. The Rosenfeld FMT overestimates the contact density, while the White-Bear version of FMT represents the simulation data accurately. In a second cut at $x = 0.5\sigma$, (b), the fluid structure, which is quite different from that at a planar wall—see figure 1—is well described by FMT. Again the White-Bear version (full line) is somewhat closer to the simulation data than the Rosenfeld FMT (dotted line).

Rosenfeld version is slightly more accurate in describing the first peak than the modifications of FMT based on more accurate equations of state. However, if one looks again at a higher packing fraction, it becomes clear that this difference is insignificant compared to the deviation between FMT and simulations—see figure 1(b) for $\eta = 0.4783$. Note that this problem persists with *all* versions of FMT, also those with tensorial weights. In the inset of figure 1(b) one can see the difference, at sufficiently high bulk densities, between the various density profiles close to contact.

The MC data of a hard-sphere fluid close to a planar hard wall are valuable benchmark data. However, it is important to realize that for this simple geometry the contact theorem, which fixes the density at the wall on the one hand and the bulk density on the other hand, clearly restricts the structure of the profile. In a more complicated geometry the differences between different versions of FMT become more pronounced, since the constraints to the density profiles close to the wall due to the contact theorem are less stringent. An example, for a hard-sphere fluid with a bulk packing fraction of $\eta = 0.3665$ in a hard wedge geometry with opening angle of 90°, is shown in figure 2. The geometry and the definition of the coordinates x and z are shown in the inset of (a). The quality of the density profile $\rho(x, z)$ was verified by comparing the density profiles of FMT predictions with MC simulations. Two cuts through the profile are shown in figure 2. The agreement between FMT and MC simulations is very good in the middle of the wedge, at $x = 0$, where the contact density is extremely high, as well as at $x = 0.5\sigma$, where the structure is still pronounced, and quite different from the structure of a hard-sphere fluid at a planar wall, as shown in figure 1. Close to contact at $z = 0.5\sigma$ there is a clear difference between the prediction of the Rosenfeld functional (dotted line) and the White-Bear version of FMT (full line). The difference between different versions of FMT are more pronounced in geometries that are more complicated, because the contact theorem is a less severe constraint there than in the planar wall case. The agreement between results of the White-Bear version of FMT and the simulation data were found to be better than those between the Rosenfeld FMT and MC [47].

For hard-sphere mixtures it is more difficult to perform a systematic comparison between FMT and simulations. Even for a binary mixture with the size ratio and two bulk densities as the only parameters, the parameter range is large and benchmark simulation data are available only for very few parameters—see e.g. [49]. The data of [49] are very well captured by FMT [29]. One example for density profiles of a binary mixture with size ratio $\sigma_b = 3\sigma_s$ and packing fractions $\eta_s = 0.0100$ and $\eta_b = 0.3576$ is shown in figure 3. Results of different versions of FMT (lines) are compared to data from MC simulations (symbols). The agreement among the different version of FMT and between FMT and MC simulations is very good. In the inset of (b) one can see small deviations between the different FMT results close to contact.

If the size ratio becomes more asymmetric, then the FMT weight functions become more troublesome, as was demonstrated by Cuesta *et al* [50], who constructed, especially for the binary case, a FMT functional with new tensorial weights. The authors compare result for the new functional to those of an earlier version [17] and concluded that despite the effort put into the new tensorial weights and the resulting higher complexity of the functional, the difference between the results of the new and simpler versions of FMT is rather negligible [50, 36].

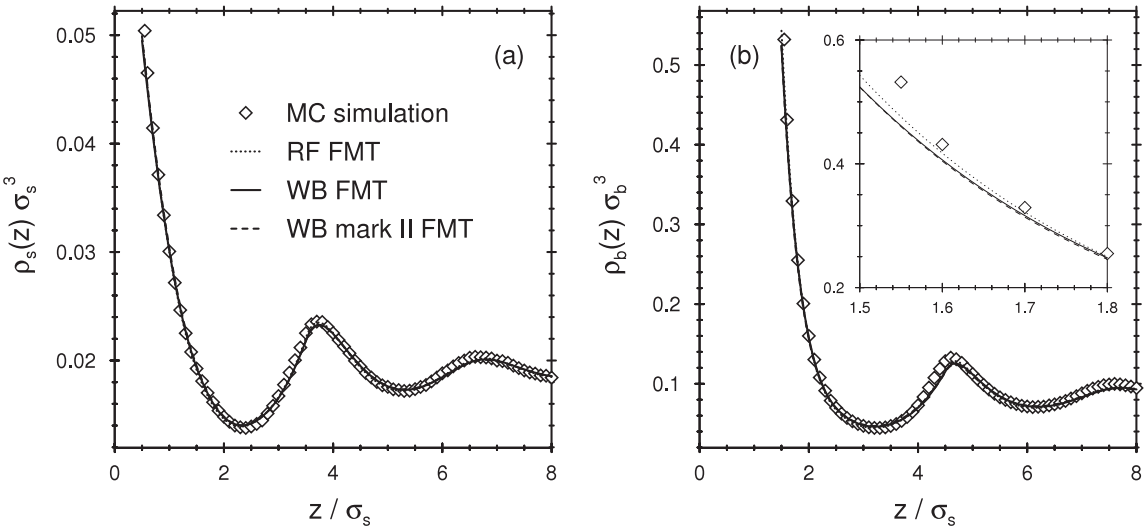

Figure 3. Density profiles at a planar hard wall of the small (a) and big (b) spheres of a binary mixture with size ratio $\sigma_b = 3\sigma_s$ and packing fractions $\eta_s = 0.0100$ and $\eta_b = 0.3576$. Contact of the small spheres and the big spheres with the wall is at $z = \sigma_s/2$, and $z = \sigma_b/2 = 3\sigma_s/2$, respectively. The predictions of different versions of FMT (lines) are compared to MC simulation data from [49]. The agreement between FMT and MC simulations (symbols) is very good. The difference between the different versions of FMT is rather small.

The phase behavior of binary hard-sphere mixtures was studied with computer simulations [51, 52]. Similar to the one-component system it was found that a binary hard-sphere mixture possesses a fluid phase and a crystal phase. If the size ratio of the small and big spheres becomes sufficiently asymmetric, there can be a fluid–fluid phase separation which, however, is always found to be meta-stable compared to fluid–crystal coexistence [51, 52].

The structure of polydisperse hard-sphere mixtures close to a planar hard wall can also be described with FMT [53].

5.1. Sum-rules

Sum-rules are statistical mechanical connections between microscopic properties of a system, such as the density profiles, and thermodynamic quantities, such as the pressure. Here I discuss two examples, which are useful for testing the internal consistency of a DFT program. The first sum-rule is the contact theorem, which connects the contact density of a fluid at a hard wall, or the inhomogeneous structure close to a soft wall, to the bulk pressure. It can be shown that the contact theorem is satisfied by WDA functionals [54, 12]. The second sum-rule is Gibbs' adsorption theorem, which connects the excess adsorption at a wall to the fluid–wall surface tension. Beside establishing connections between different quantities, these sum-rules are of great practical importance, because they allow one to test whether a DFT implementation can correctly compute both density profiles and thermodynamic quantities.

The contact theorem at a planar wall, modeled by external potentials $V^i_{\rm ext}(z) = V^i_{\rm ext,hw}(z) + V^i_{\rm ext,soft}(z)$ with hard wall parts, $V^i_{\rm ext,hw}(z)$, and soft parts, $V^i_{\rm ext,soft}(z)$, is given by

$$\sum_i \rho_i(z = R_i^+) = \beta p - \sum_i \int {\rm d}z\, \rho_i(z) \frac{{\rm d}\beta V^i_{\rm ext,soft}(z)}{{\rm d}z}, \quad (26)$$

where $\rho_i(z = R_i^+)$ denote the densities of species i at contact with the wall and the derivative on the r.h.s. acts only on the soft part of the external potentials—the derivative of the hard wall potentials $V^i_{\rm ext,hw}$ gave rise to Dirac-delta distributions, which are accounted for by the l.h.s. of equation (26). If the wall is hard, then the integral over the density profile on the r.h.s. of equation (26) vanishes and the contact theorem simplifies to the sum over the contact densities, which equals the bulk pressure. If the wall is soft, without a hard core, then the sum over the contact densities vanishes on the l.h.s. of equation (26).

Depending on the version of FMT, the underlying bulk pressure differs. This in turn influences the inhomogeneous structure close to the wall. The PY equation of state is less accurate than the MCSL pressure. Equation (25) for mixtures is more accurate than the MCSL pressure. Besides the accuracy of the underlying equation of state, compared to computer simulations, the contact theorem can be employed to verify if a DFT implementation can correctly compute the structure, because equation (26) can only be satisfied for various external potentials and at various values of bulk densities, if the density profiles numerically calculated by minimizing the DFT are correct. Without too much numerical effort, the contact theorem can be satisfied to 4 significant figures. With some additional effort, a better agreement is also possible.

Generalization of the contact theorem to spherical or cylindrical geometry is straightforward [57–59].

The Gibbs adsorption theorem connects the excess adsorption Γ_i of species i with the derivative of the surface tension γ w.r.t. the chemical potential of species i:

$$\Gamma_i = \int {\rm d}z\, (\rho_i(z) - \rho_i^{\rm bulk}) = -\left(\frac{{\rm d}\gamma}{{\rm d}\mu_i}\right)_{V,T}, \quad (27)$$

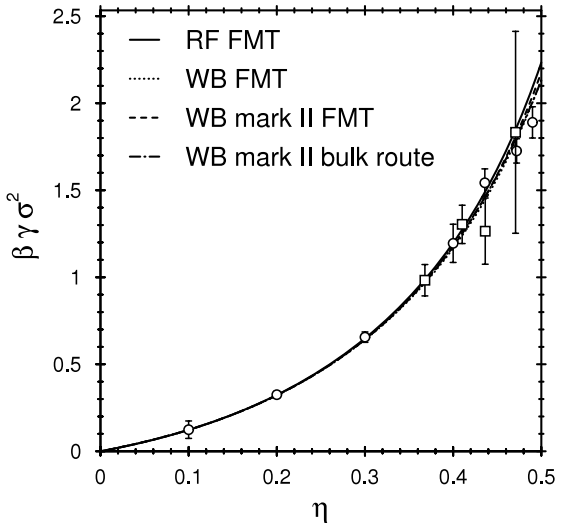

Figure 4. The wall surface tension of a hard-sphere fluid at a planar hard wall as a function of the bulk packing fraction η. Numerical FMT results (full, dashed, and dotted lines) and analytic results from the bulk route (dashed–dotted line) are compared to computer simulations from Heni *et al* [55] (circles) and from Henderson *et al* [56] (squares). There is very good agreement between FMT and simulations. The difference between the different FMT results is rather small and the simulation data do not allow one to differentiate clearly between the approaches.

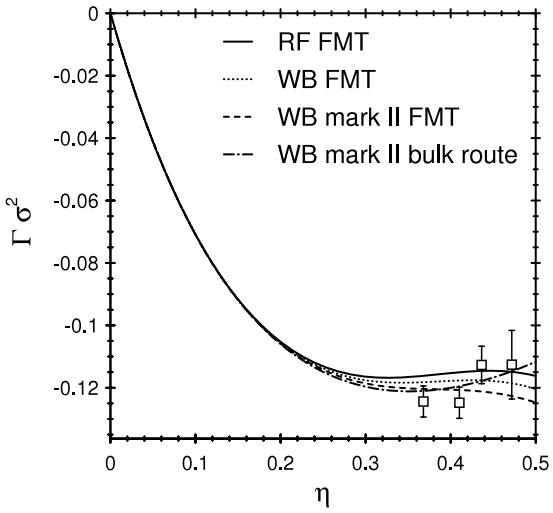

Figure 5. The excess adsorption of a hard-sphere fluid at a planar hard wall as a function of the bulk packing fraction η. Numerical FMT results (full, dashed, and dotted lines) and analytic results from the bulk route (dashed–dotted line) are compared to computer simulations from Henderson *et al* [56] (squares). The difference between the different FMT results is larger than those for the wall surface tension γ, but still the simulation data do not allow one to differentiate clearly between the approaches. The lines were calculated from the density profiles and agree very well with the excess adsorption obtained from Gibbs' adsorption theorem.

with the wall surface tension, which is defined by

$$\gamma = \frac{1}{A}(\Omega + pV). \tag{28}$$

Note that the wall surface tension is *not* uniquely defined, but rather depends on the definition of the system volume V. If the system volume is defined as the volume accessible to the centers of the spheres, i.e. starting at $z = R_i$ (see figure 1), then the wall surface tension of a pure hard-sphere fluid is negative and the resulting excess adsorption is positive. Note that this definition, which is often used in the literature for the pure hard-sphere fluid, can be problematic in the case of mixtures, since the centers of different species have different volumes available. If the system volume V starts at $z = 0$, which is independent of the particle size in the case of hard-sphere mixtures and which is the definition used here, then the surface tension is positive and the corresponding excess adsorption is negative. The wall surface tension, according to this definition for a pure hard-sphere fluid, is shown in figure 4. FMT results (lines) are compared to computer simulations from Heni *et al* [55] (circles) and from Henderson *et al* [56] (squares). The simulation data from Henderson *et al* had to be transformed to the volume definition used here. The agreement between FMT and simulation data is excellent. Unfortunately this comparison does not allow one to decide which version of FMT is most accurate.

Combining ideas from SPT [8] and morphological thermodynamics [60] it is possible to obtain an analytic approximation of the wall surface tension for a hard-sphere mixture at a planar hard wall. One finds [47]

$$\beta\gamma = \frac{\partial\Phi}{\partial n_2},$$

which is also valid for mixtures [61]. For the bulk excess free energy of the White-Bear version of FMT mark II [46] the resulting approximation is shown in figure 4 as a dashed–dotted line. The agreement with numerical FMT results and with simulation data is very good.

Note that since the wall surface tension and the excess adsorption are not experimentally measurable, the definition of the system volume is arbitrary. Especially for the one-component fluid, both definitions aforementioned are equivalent and results from one definition can easily be translated into the other definition. However, in order for the adsorption theorem to be satisfied it is essential that the volume V in equation (28) has to coincide with the area A times the integration range in equation (27).

In figure 5 the excess adsorption, obtained from the density profiles, of a pure hard-sphere fluid at a planar hard wall is shown as a function of the bulk packing fraction η. FMT results (lines) are compared to computer simulation data from Henderson *et al* [56] (squares). The small difference between FMT results in the wall surface tension are more pronounced in the excess adsorption. Unfortunately, it is not possible to clearly decide which FMT result is most accurate.

Using the analytic approximation of the wall surface tension it is straightforward to calculate the excess adsorption within the same bulk route:

$$\Gamma_i = -\frac{\partial}{\partial\beta\mu_i}\left(\frac{\partial\Phi}{\partial n_2}\right).$$

Table 1. Coexisting densities and the pressure at coexistence of a one-component hard-sphere fluid and its crystal obtained from different versions of FMT. While a modification of the original Rosenfeld FMT, such as the empirical one given in equation (18), denoted as Rosenfeld-$q3$, or the tensor weighted densities are necessary to obtain a stable hard-sphere crystal, the coexisting fluid (f) and solid (s) density, ρ_f and ρ_s, respectively, and the pressure at coexistence βp_{coex} depend sensitively on the underlying thermodynamics. For the PY equation of state, denoted by Rosenfeld-tensor [17, 18, 20], the coexisting densities are somewhat removed from the simulation data, while for the CS equation of state, denoted by White-Bear-tensor [18–20], the agreement with simulations is good. Interestingly, the coexisting densities of the Rosenfeld-$q3$ version [16] are even closer to the simulation results.

Approach	$\rho_f\sigma^3$	$\rho_s\sigma^3$	$\beta p_{coex}\sigma^3$
Simulation Hoover *et al* [21]	0.940	1.040	11.7
Simulation Noya *et al* [22]	0.938	1.037	11.54
Rosenfeld-tensor [17, 18, 20]	0.892	0.985	9.9
Rosenfeld-$q3$ [16]	0.938	1.037	12.3
White-Bear-tensor [18–20]	0.934	1.023	11.3

For a one-component hard-sphere fluid the prediction of the bulk route using the excess free energy density of the White-Bear version of FMT mark II is shown in figure 5 as a dashed–dotted line. The agreement with the numerical results and with simulation data is good.

To check the validity of the implementation of the FMT program, I also verified that Gibbs' adsorption theorem is satisfied, i.e. the integral over the density profiles agrees with the derivative of the wall surface tension w.r.t. the chemical potential. A small error in the calculation of the density profiles or of the wall surface tension would result in a violation of equation (27).

6. Properties of the crystal

Beside bulk and inhomogeneous fluids, it is possible to study properties of the hard-sphere crystal within the framework of FMT. Other than a free minimization of the density profile, which is employed to determine the structure of the fluid phase, the crystal is usually studied using a parameterized density profile. For a one-component hard-sphere (bulk) solid the usual Gaussian form of the density profile is given by [62]

$$\rho(\mathbf{r}) = \left(\frac{\alpha}{\pi}\right)^{\frac{3}{2}} \sum_{\{\vec{R}\}} \mathrm{e}^{-\alpha(\vec{r}-\vec{R})^2}, \qquad (29)$$

with the mean peak width $\alpha^{-1/2}$. The sum in equation (29) is taken over all points $\{\vec{R}\}$ of the lattice. Clearly the lattice symmetry is an input to this approach. In the case of a hard-sphere crystal the symmetry is known to be fcc.

For Gaussian peaks it is possible to calculate the weighted densities analytically [16], which can be inputted into an appropriate FMT functional, i.e. either an anti-symmetrized functional, equation (18), or one with tensor weights, equation (20). The grand potential functional with vanishing external potential at a given μ is minimized with respect to both the lattice size and the Gaussian parameter α. From the minimization the properties of the hard-sphere solid, such as the equation of state or the peak width $\alpha^{-1/2}$, follow. In addition it is possible to determine the coexisting densities ρ_f and ρ_s between the hard-sphere fluid (f) and solid (s).

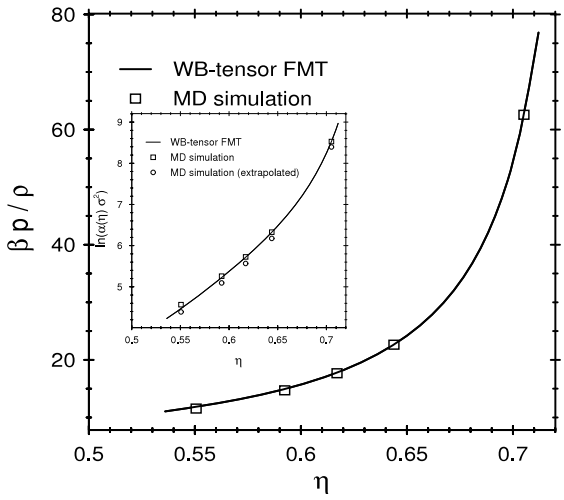

Figure 6. The equation of state $\beta p/\rho$, and in the inset the Gaussian parameter α, of the hard-sphere fcc solid as a function of the packing fraction η. The full lines denote the results of the White-Bear-tensor version of FMT. The FMT results for the equation of state compare well with MD results for 500 particles (squares) [63], and those for the Gaussian parameter α compare well with MD results for 500 particles (squares) and extrapolations to $N \to \infty$ (circles) [64].

In table 1 the densities of the coexisting fluid, ρ_f, and solid, ρ_s, from different versions of FMT are compared to the classic simulation results of Hoover *et al* [21] and more recent data by Noya *et al* [22]. Tarazona's modification [17] with tensor weighted densities of the original Rosenfeld FMT, can describe the hard-sphere solid. Its underlying thermodynamics corresponds to the Percus–Yevick results, which becomes inaccurate at higher densities. Accordingly, the coexisting densities and the pressure at coexistence differ significantly from the simulation data [18, 20]. The Rosenfeld-$q3$ functional, equation (18) with $q = 3$, also builds on PY thermodynamics. Surprisingly, the coexisting densities obtained by this functional [16] are in very good agreement with simulations. The pressure at coexistence, however, is clearly overestimated. Using the White-Bear version of FMT with tensor weights the agreement of the calculated coexisting densities and the pressure at coexistence with simulations, especially the more recent ones [22], is very good [18–20].

The agreement between DFT and MD results for the equation of state of the solid is excellent, as shown in figure 6. The full line denotes results of the White-Bear-tensor results and the symbols those from MD computer simulations [63] for 500 particles.

The Gaussian parameter α, as a function of the packing fraction η, is directly obtained from the minimization of the functional. It is shown in the inset of figure 6. The agreement between the DFT results and the MD data for 500 particles (squares) and data extrapolated to $N \to \infty$ (circles) of [64] is very good. The equation of state and the Gaussian parameter based on Tarazona's Rosenfeld-tensor functional are almost identical with the results shown in figure 6.

Clearly, it is possible to improve the description of the solid in various ways. For example, the parameterization of the density profile in equation (29) can be improved by replacing the Gaussian with a general, spherical symmetric function $f(r)$. Groh *et al* [65, 66] did this and minimized the functional in order to determine $f(r)$. Tarazona took effects of anisotropy in the density profile of the solid into account [17] and thereby improved the simple form given in equation (29) in a different way. A free minimization of FMT for the density profile of a crystal, as was performed for a different WDA functional [67], is still missing. Lutsko studied hard-sphere crystals with bcc and sc symmetry, beside the usual fcc crystal [68].

The crystal of a binary hard-sphere mixture with size ratios between $\sigma_s/\sigma_b = 0.95$ and 0.85 was recently studied within FMT using a Gaussian parameterization for the density profiles [69]. The size ratios considered are chosen with a reference system for interacting systems in mind. Several interesting features found in simulations of binary mixtures with highly asymmetric size ratios have not been addressed with FMT functionals yet.

7. FMT approaches for other models

While the focus of this review is on the FMT for hard-sphere mixtures, it is important to mention at least a few developments for other systems that were inspired by it. Since this section is short, it has to remain incomplete and can give only a taste of the several branches of the theory of fluids and colloidal mixtures that were influenced by Rosenfeld.

The ideas leading to FMT in $d = 3$ can also be applied in $2d$. Rosenfeld derived a FMT functional for mixtures of hard-disks [70], which is different from the two-dimensional limit of the hard-sphere functional. While Rosenfeld employed the same strategy, one important difference between two- and three dimensions is that in even dimensions the deconvolution of the Mayer-f function can only be performed approximately. A similar problem arises for non-spherical particles [38, 39, 37].

Cuesta showed that a FMT functional for parallel hard cubes can be constructed using the FMT structure [71], which helps to study packing effects and sheds some new light on FMT. One interesting development based on the FMT for parallel hard cubes is the formulation of a lattice FMT functional [72].

If the hard-sphere interactions are replaced by a step-like repulsive pair interaction

$$V_{ij}(r) = \begin{cases} \epsilon & r < R_i + R_j \\ 0 & \text{otherwise,} \end{cases}$$

it seems at first that FMT should be able to cope with this system equally well as with the hard spheres. After all the Mayer-f function is still a step function. Schmidt solved the problem [73] starting from the $0d$ limit of the problem, and he found that the modification in the pair interactions changes the functional more than first expected.

Schmidt also derived FMT functionals for various models of non-additive hard-sphere mixtures. The first functional was for a model colloid–polymer mixture [35] within the Asakura–Oosawa model [74, 75] with hard-sphere interactions among colloids (c) and between a colloid and a polymer (p),

$$V_{cc}(r) = \begin{cases} \infty & r < 2R_c \\ 0 & \text{otherwise} \end{cases}$$

and

$$V_{cp}(r) = \begin{cases} \infty & r < R_c + R_p \\ 0 & \text{otherwise,} \end{cases}$$

while the polymer–polymer interaction vanishes, $V_{pp}(r) = 0$. At low polymer concentration, the system behaves essentially like hard spheres. At higher concentrations, however, if the polymer is not too small, the system can undergo a phase separation into a colloid-rich and a colloid-poor fluid. The functional was first derived from the $0d$ limit [35], but it was later shown [76] that the functional could be derived by linearizing a functional for hard-sphere mixtures in the density of the polymer. The functional for the model colloid–polymer mixture was found to predict layering and wetting transitions at a planar hard wall [77, 78] and allows one to study the free interface between a colloid-rich and colloid-poor fluid phase [78].

Schmidt also constructed a functional for the Widom–Rowlinson model [79], which employs the pair interactions

$$V_{ii}(r) = 0 \quad \text{and} \quad V_{i\neq j}(r) = \begin{cases} \infty & r < R_i + R_j \\ 0 & \text{otherwise,} \end{cases}$$

which also displays a phase separation into two fluid phases. The FMT functionals for the penetrable spheres, for the model colloid–polymer mixture and for the Widom–Rowlinson model all have a structure and level of complexity similar to that of the hard-sphere functionals. The general case of a binary hard-sphere mixture with non-additive diameter σ_{11}, σ_{22}, and

$$\sigma_{12} = \tfrac{1}{2}(\sigma_{11} + \sigma_{22})(1 + \Delta)$$

with $\Delta \neq 0$ is significantly more complex and was also derived by Schmidt [80]. The functional makes use of weight functions that include derivatives of Dirac-delta distributions up to fifth order and a matrix kernel for the free energy.

There are also developments inspired by FMT that make use of the fact that FMT is a mixture theory. The calculation of depletion potentials in hard-sphere mixtures using the insertion route [81] is very efficient, but requires a DFT for mixtures. The insertion route can be applied to polydisperse systems [82], for the calculation of three-body depletion interactions [83], and interestingly, also to compute the depletion potential in non-additive hard-sphere mixtures using the functional for additive hard-sphere mixtures [84].

The FMT functional for the model colloid–polymer mixture [35] allows one to make contact with SPT, one of the starting points of FMT. The central quantity of SPT is the reversible work required to create a cavity in a fluid, large enough to hold a particle [8]. This work can be connected to the excess chemical potential and therefore be connected to FMT [85].

8. Implementation

In this section I briefly discuss a few details about the implementation of a FMT functional. One important part of the numerical implementation is the algorithm that minimizes the functional. In section 8.1 I present a simple, yet robust scheme based on the Piccard iteration. I highlight the structure of FMT in two common geometries with planar and spherical symmetry in sections 8.2 and 8.3, respectively. In these geometries the calculation of the weighted densities can be expressed in terms of one-dimensional convolutions, which can be calculated efficiently in Fourier space. I present a way to increase the accuracy of the computation of convolution in Fourier space in section 8.4.

In the fluid phase, the inhomogeneous density profiles share spatial symmetry with the external potentials. For example, if the fluid is confined by planar walls (either a single wall or a slit) then the external potentials depend only on the distance perpendicular to the walls, which is denoted here by z. In this case the density profiles also depend solely on z. In the calculation of weighted densities the integration over the other coordinates can be performed analytically so that the three-dimensional convolutions in equation (6) can be reduced to one-dimensional integrations. In the case of planar and spherical geometry, the cases discussed in the following, these one-dimensional integrations remain convolutions, which allows for their evaluation in Fourier space. In cylindrical geometry, however, one loses the convolution property by performing two integrals analytically.

For the minimization of the density functional it is also important to calculate the variations of the functional w.r.t. the density profiles. In general, one obtains

$$\frac{\delta\Omega[\{\rho_i\}]}{\delta\rho_i(\mathbf{r})} = \frac{\delta\mathcal{F}_{\mathrm{ex}}[\{\rho_i\}]}{\delta\rho_i(\mathbf{r})} + \beta^{-1}\ln\lambda_i^3\rho_i(\mathbf{r}) + V_{\mathrm{ext}}^i(\mathbf{r}) - \mu_i = 0. \tag{30}$$

The variation of the excess free energy can be performed using the structure of FMT

$$c_i^{(1)}(\mathbf{r}) = -\beta\frac{\delta\mathcal{F}_{\mathrm{ex}}[\{\rho_i\}]}{\delta\rho_i(\mathbf{r})} = -\sum_\alpha\int \mathrm{d}\mathbf{r}'\,\frac{\partial\Phi(\{n_\alpha\})}{\partial n_\alpha}\frac{\delta n_\alpha(\mathbf{r}')}{\delta\rho_i(\mathbf{r})},$$

with the one-body direct correlation function of species i, $c_i^{(1)}(\mathbf{r})$.

8.1. Piccard iteration

The functional $\Omega[\{\rho_i(\mathbf{r})\}]$ and the one-body direct correlation function $c_i^{(1)}(\mathbf{r})$ are all ingredients required for a minimization of the functional using a simple Piccard iteration scheme. This is a simple but robust algorithm. One starts with an initial guess for the density profiles $\rho_i^{(j=0)}(\mathbf{r})$, at iteration step $j = 0$, and iterates the profiles until $\rho_i^{(j)}(\mathbf{r})$ or the grand potential $\Omega[\{\rho_i^{(j)}(\mathbf{r})\}]$ no longer change according to a threshold criterion.

Of course, there are more sophisticated algorithms, e.g. based on a pseudo Newton algorithm [86, 87]. However, they typically require the second variation of the functional w.r.t. density profiles and will not be discussed here.

First the density profiles have to be initialized. One simple choice is to set $\rho_i^{(j=0)}(\mathbf{r}) = \rho_{\mathrm{bulk}}^i$, wherever the external potential allows a non-vanishing density. If the attractive parts of the external potential are not too strong, one could also start with the ideal gas solution $\rho_i^{(j=0)}(\mathbf{r}) = \rho_{\mathrm{bulk}}^i\exp(-\beta V_{\mathrm{ext}}^i(\mathbf{r}))$. For strong attraction, however, this could easily lead to local packing fractions close to or above 1, which are unphysical.

Using the guess of the density profiles at iteration step j, $\rho_i^{(j)}(\mathbf{r})$, one can solve equation (30) formally to find [1]

$$\tilde{\rho}_i^{(j)}(\mathbf{r}) = \rho_{\mathrm{bulk}}^i\exp(-\beta V_{\mathrm{ext}}^i(\mathbf{r}) + c_i^{(1)}(\mathbf{r}) + \beta\mu_{\mathrm{ex}}^i).$$

Note that for this step the chemical potentials have been split into the ideal gas contributions, which give rise to the prefactor ρ_{bulk}^i to the exponential, and the excess contributions μ_{ex}^i. If the input density profiles $\rho_i^{(j)}(\mathbf{r})$ are close to the equilibrium profiles, then $\tilde{\rho}_i^{(j)}(\mathbf{r})$ will also be close to the equilibrium profiles. However, especially at the start of the iteration, when the input density profiles are far from the equilibrium ones, $\tilde{\rho}_i^{(j)}(\mathbf{r})$ can be quite rough approximations.

In order to moderate the iteration and to prevent the procedure from diverging, it proves useful to mix the input profiles with $\tilde{\rho}_i^{(j)}(\mathbf{r})$ using a mixing parameter α

$$\rho_i^{(j+1)}(\mathbf{r}) = (1-\alpha)\rho_i^{(j)}(\mathbf{r}) + \alpha\tilde{\rho}_i^{(j)}(\mathbf{r}).$$

It is important to choose $\alpha \in [0, 1]$ large enough to allow for fast convergence, but also sufficiently small to prevent instabilities in the iteration procedure.

It turns out that a *smart* choice of the mixing parameter is very helpful. Here I describe a simple, yet powerful tweak of the iteration scheme in order to improve the convergence.

There are two factors which limit the value of the mixing parameter α. On the one hand, especially at the beginning of the iteration, when the density profiles are far from the equilibrium profiles, α has to be small in order to prevent the local packing fraction $n_3(\mathbf{r})$ *after* mixing from exceeding 1—a value of n_3 larger than 1 would clearly cause problems in terms like $\ln(1-n_3)$ or $1/(1-n_3)$. On the other hand α should be sufficiently large so that the functional of the grand potential decreases after mixing. Both factors can be taken into account by two steps. In the first step the smallest value of $\alpha \in [0, 1]$ is determined that would cause $n_3(\mathbf{r})$ to become 1 (if possible) after mixing. Since $n_3(\mathbf{r})$ before the mixing and $\tilde{\rho}_i(\mathbf{r})$ are known this can be done easily. Once the maximum of the mixing parameter, $\alpha_{\max}$ is determined, one can *guess* the optimal mixing parameter, α_{opt}. For practical purposes it proves useful to restrict the value of α_{opt} to the interval $[0, 0.9\alpha_{\max}]$. In figure 7 the full and the dashed vertical lines mark $\alpha_{\max}$ and $0.9\alpha_{\max}$, respectively. In the second step α_{opt} is guessed from the behavior of the grand potential as a function of the mixing parameter. $\Omega_1 = \Omega(\alpha = 0)$ is known from the last iteration step. While sophisticated line-search algorithms are available for this problem, one should avoid too many evaluations of the functional of the grand potential, which also include the calculations of the weighted densities. To this end one can make half of the maximal step, i.e. evaluate $\Omega_2 = \Omega(0.45\alpha_{\max})$. If the functional of the grand potential

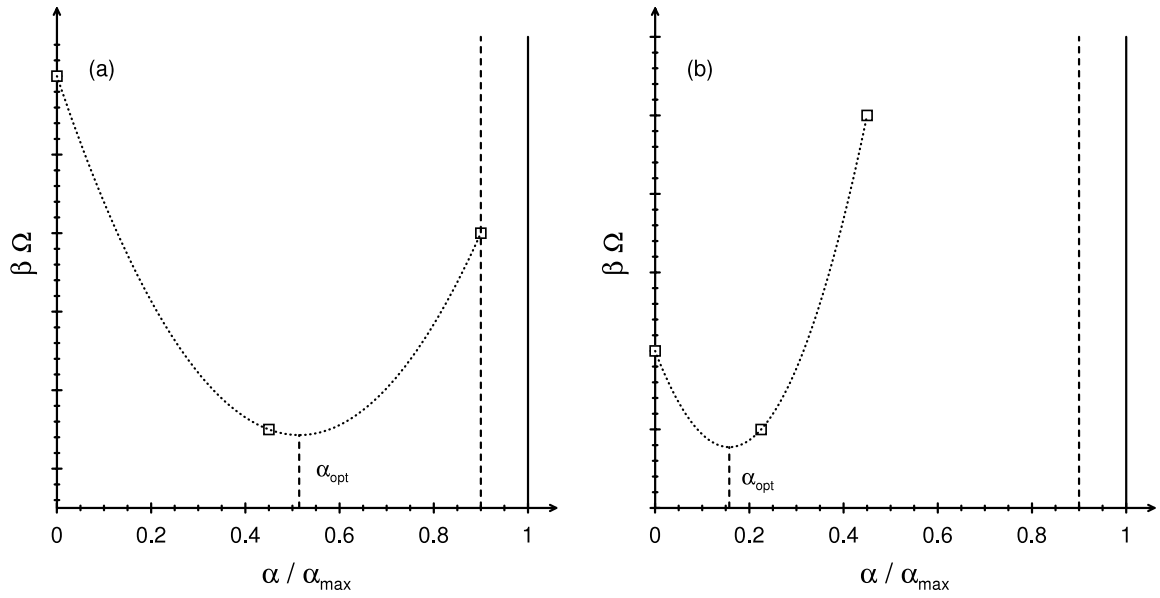

Figure 7. The mixing parameter α for the Piccard iteration has to be smaller than $\alpha_{\max}$ (full vertical line) and is chosen in the interval $[0, 0.9\alpha_{\max}]$ so that $\Omega(\alpha)$ decreases. If $\Omega(0.45\alpha_{\max}) < \Omega(0)$, (a), then also $\Omega(0.9\alpha_{\max})$ is evaluated. If $\Omega(0.45\alpha_{\max}) > \Omega(0)$, (b), then $\Omega(0.225\alpha_{\max})$ is evaluated. A quadratic fit through these three data points allows one to *guess* $\alpha_{\rm opt}$, the optimal value of the mixing parameter.

decreased, i.e. $\Omega_2 \leqslant \Omega_1$, then one also evaluates the functional for the maximal step site $\Omega_3 = \Omega(0.9\alpha_{\max})$, as depicted in figure 7(a), otherwise, if $\Omega_2 > \Omega_1$ one makes a smaller step $\Omega_3 = \Omega(0.225\alpha_{\max})$, as shown in figure 7(b). Assuming a quadratic form for $\Omega(\alpha)$ (dotted lines in figure 7) one can *guess* $\alpha_{\rm opt}$ from fitting a quadratic polynomial to Ω_i, $i = 1, 2, 3$ and calculating that value of α that minimizes this quadratic form.

8.2. Planar geometry

For the weighted densities in planar geometry one finds that

$$n_\alpha(\mathbf{r}) = n_\alpha(z) = \sum_i \int \mathrm{d}z'\, \rho_i(z')\, \omega_\alpha^i(z - z') \qquad (31)$$

with z the distance perpendicular to the wall. The *one-dimensional* weight functions are $\omega_3^i(z) = \pi(R_i^2 - z^2)\Theta(R_i - |z|)$, $\omega_2^i(z) = 2\pi R_i \Theta(R_i - |z|)$, and $\vec{\omega}_2^i(z) = 2\pi z \vec{e}_z \Theta(R_i - |z|)$, with the unity vector in the direction normal to the wall $\vec{e}_z$. The remaining weight functions are related to $\omega_2^i(z)$ and $\vec{\omega}_2^i(z)$ via $\omega_1^i(z) = \omega_2^i(z)/(4\pi R_i)$, $\omega_0^i(z) = \omega_2^i(z)/(4\pi R_i^2)$, and $\vec{\omega}_1^i(z) = \vec{\omega}_2^i(z)/(4\pi R_i)$.

From the definition of the one-body direct correlation function and the structure of the excess free energy functional within fundamental measure theory one obtains

$$c_i^{(1)}(z) = -\beta \frac{\delta \mathcal{F}_{\rm ex}[\{\rho_i\}]}{\delta \rho_i(z)} = -\sum_\alpha \int \mathrm{d}z' \, \frac{\partial \Phi(\{n_{\tilde{\alpha}}\})}{\partial n_\alpha} \frac{\delta n_\alpha(z')}{\delta \rho_i(z)}.$$

The main problem is to calculate the variation of the weighted densities $n_\alpha(z')$ w.r.t. the density profile $\rho_i(z)$. The result (in planar geometry) is quite simple

$$\frac{\delta n_\alpha(z')}{\delta \rho_i(z)} = \frac{\delta}{\delta \rho_i(z)} \sum_j \int \mathrm{d}z''\, \rho_j(z'') \omega_\alpha^j(z' - z'') = \omega_\alpha^i(z' - z).$$

However, one has to be careful because, compared to the argument entering the weight function of the weighted densities, equation (31), the argument entering the calculation of $c_i^{(1)}(z)$ is negative, i.e. $z - z'$ becomes $z' - z$. For the scalar weight functions this is unimportant, since the scalar weight functions are even functions

$$\omega_\alpha^i(z' - z) = \omega_\alpha^i(z - z'),$$

but the vector-like weight functions are odd functions

$$\vec{\omega}_\alpha^i(z' - z) = -\vec{\omega}_\alpha^i(z - z').$$

Taking this sign into account, it is possible to perform the convolutions in Fourier space using FFT methods:

$$c^{(1)}(z) = -\sum_\alpha \mathcal{F}T^{-1}\left(\mathcal{F}T\left(\frac{\partial \Phi(\{n_{\tilde{\alpha}}\})}{\partial n_\alpha} \right) * \mathcal{F}T(\pm\omega_\alpha) \right),$$

where $\mathcal{F}T$ and $\mathcal{F}T^{-1}$ denote the fast Fourier transform and its inverse, respectively.

8.3. Spherical geometry

If the external potential is spherical symmetric and the fluid phase is considered, then the density profiles and the weighted densities depend only on the radial distance r. Here only the case $r > R_i$, $i = 1, \ldots, \nu$ is considered, for which the *scalar* weighted densities are given by

$$n_\alpha(\mathbf{r}) = n_\alpha(r) = \frac{1}{r} \sum_i \int \mathrm{d}r'\, \rho_i(r') r' \omega_\alpha^i(r - r').$$

The *one-dimensional scalar* weight functions are $\omega_3^i(r) = \pi(R_i^2 - r^2)\Theta(R_i - r)$, $\omega_2^i(r) = 2\pi R_i \Theta(R_i - r)$, $\omega_1^i(r) = \omega_2^i(r)/(4\pi R_i)$, and $\omega_0^i(r) = \omega_2^i(r)/(4\pi R_i^2)$ are basically the

same as in planar geometry. The vector weighted densities are somewhat more complicated:

$$\begin{aligned}\vec{n}_2(r) &= -\vec{e}_r \frac{\partial}{\partial r} n_3(r) \\ &= \left\{ \frac{n_3(r)}{r}\vec{e}_r - \frac{1}{r}\sum_i \int \mathrm{d}r'\, \rho_i(r') r' \vec{\omega}_2^i(r-r') \right\} \\ &= \left\{ \frac{1}{r^2}\sum_i \int \mathrm{d}r'\, \rho_i(r') r' \omega_3^i(r-r')\vec{e}_r \right. \\ &\quad \left. - \frac{1}{r}\sum_i \int \mathrm{d}r'\, \rho_i(r') r' \vec{\omega}_2^i(r-r') \right\}\end{aligned}$$

with the unit vector in radial direction $\vec{e}_r$ and the weight function $\vec{\omega}_2^i(r) = 2\pi r \vec{e}_r \Theta(R_i - r)$. The second vector weighted density follows directly

$$\begin{aligned}\vec{n}_1(r) = \left\{ \frac{1}{r^2}\sum_i \int \mathrm{d}r'\, \rho_i(r') r' \frac{\omega_3^i(r-r')}{4\pi R_i}\vec{e}_r \right. \\ \left. - \frac{1}{r}\sum_i \int \mathrm{d}r'\, \rho_i(r') r' \frac{\vec{\omega}_2^i(r-r')}{4\pi R_i} \right\}.\end{aligned}$$

The vector weighted densities are a sum of two convolutions. Note the factor $1/r^2$ in front of the first term.

For the calculation of the one-body direct correlation function, one has again to distinguish between scalar and vector weighted densities. The scalar terms can be treated in an analogous way to those in the planar geometry. The vector weighted density requires a bit more care, because in the variation of the weighted density w.r.t. the density the first term possesses a factor $1/r^2$ and an even weight function and the second term a factor $1/r$ and an odd weight function.

8.4. Convolutions in Fourier space

In planar and in spherical geometry the calculation of the weighted densities and the one-body direct correlation function can be reduced to a sum of one-dimensional convolution integrals. This implies that their computation can be done using the convolution theorem in Fourier space. The use of fast Fourier transforms (FFT) can speed up the calculation considerably. However, it is important to note that the direct use of FFT methods for the calculation of the convolution of two functions, say $f(x)$ and $g(x)$, results in

$$\begin{aligned}\int_{x_1}^{x_N} \mathrm{d}x\, f(x')g(x'-x) &\approx \mathcal{FT}^{-1}(\mathcal{FT}(f) * \mathcal{FT}(g)) \\ &= \Delta x \sum_{j=1}^{N} f_j g_{i-j},\end{aligned}$$

which corresponds to a very simple quadrature formula. In real space the implementation of more accurate quadrature formulae would be straightforward, i.e. by applying a closed extended formula, [88]

$$\begin{aligned}\int_{x_1}^{x_N} \mathrm{d}x\, f(x')g(x'-x) = \Delta x(&\tfrac{3}{8}f_1 g_{i-1} + \tfrac{7}{6}f_2 g_{i-2} \\ &+ \tfrac{23}{24}f_3 g_{i-3} + f_4 g_{i-4} + \cdots + f_{N-3} g_{i-N+3} \\ &+ \tfrac{23}{24}f_{N-2} g_{i-N+2} + \tfrac{7}{6}f_{N-1} g_{i-N+1} + \tfrac{3}{8}f_N g_{i-N}) \end{aligned} \quad (32)$$

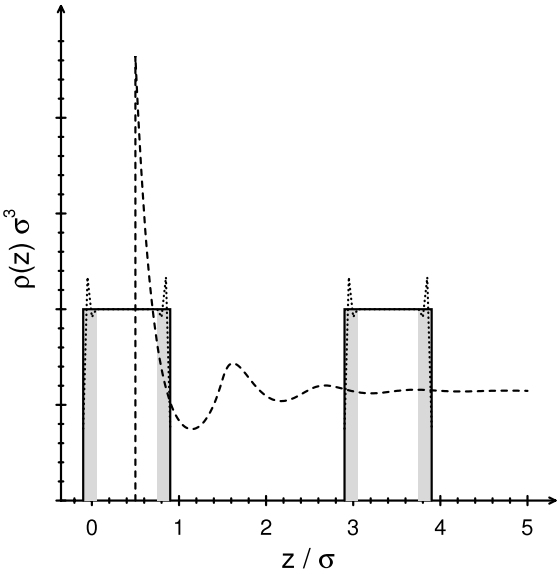

Figure 8. The convolution of a density profile (dashed line) with a weight function (full line) or the modified weight function (dotted line). The modification of the weight function, highlighted by the gray shaded area, increases the accuracy of the convolution computed in Fourier space. However, in the case of a hard wall, where the density profile jumps discontinuously to zero, as shown in this figure, special care is required for small distances from the wall. As indicated by the modified weight function, that only partly overlaps with the density profile, the modification (gray area) on the left does not contribute to the convolution since it is convolved with a part of the density profile that vanishes. In the region $z < 2R_i$ the modified convolution has to be *corrected*.

with an error of the order $\mathcal{O}(\Delta x)^4$. Here, however, the aim is an implementation in Fourier space. Note that the convolutions are products between weight functions with a short range and a function with a range that is confined only by the geometry defined by the external potential, i.e. the density profiles or the derivatives of the excess free energy density w.r.t. a weighted density. This is shown in figure 8. It seems natural to adapt equation (32) in Fourier space by modifying the *effective one-dimensional* weight functions at the boundaries of their range by

$$\tilde{\omega}_\alpha^i(x = \pm R_i) = \tfrac{3}{8}\omega_\alpha^i(x = \pm R_i)$$

$$\tilde{\omega}_\alpha^i(x = \pm(R_i - \Delta x)) = \tfrac{7}{6}\omega_\alpha^i(x = \pm(R_i - \Delta x))$$

$$\tilde{\omega}_\alpha^i(x = \pm(R_i - 2\Delta x)) = \tfrac{23}{24}\omega_\alpha^i(x = \pm(R_i - 2\Delta x))$$

while leaving it unchanged otherwise. This modification in the gray shaded area, indicated by the dotted line as compared to the original weight function denoted by the full line in figure 8, has the advantage that the convolution is as fast as the original convolution *but* more accurate. However, if density profiles at a hard wall are considered, then the convolution product between density profiles and weight functions has to be slightly modified in the range close to the wall, because the density profiles vanish discontinuously at the wall, as shown in one case in figure 8.

9. Conclusion

FMT is an elegant and powerful approach to DFT for hard spheres, as I have hopefully convinced the reader with this review. Based on the insight that for hard spheres the Mayer clusters have a purely geometrical meaning, Rosenfeld used weight functions that correspond to the fundamental geometrical measures of individual spheres and thereby created an approach that can account not only for pure systems but also for mixtures.

I have reviewed three different approaches to FMT: first Rosenfeld's original approach that, based on ideas from SPT and PY integral equation theory, resulted in a functional that could successfully describe fluid properties, but failed to account for the freezing transition. The second approach, based on the insight of dimensional crossover, corrected the problem with freezing. The third approach, based on accurate mixture equations of state, improved the thermodynamics underlying FMT.

FMT is successful and accurate in describing the inhomogeneous structure of hard-sphere fluids and solids, and corresponding thermodynamic quantities. In this review I have described several tests for the accuracy of both the structure and thermodynamic quantities, such as the wall surface tension and the excess adsorption at a planar hard wall. There are small deviations between the results of different versions of FMT. However, present simulation results do not allow one to clearly decide which result is most accurate.

I have concluded the review with a few hints on the implementation of FMT. These hints are hopefully useful both for readers new to FMT as well as to those with some experience.

This review has focused on FMT for hard-sphere mixtures. I have briefly mentioned some closely related approaches for spherical particles in section 7. There are also interesting developments for non-spherical hard particles, which I did not discuss here. Interested readers are referred to [36].

FMT provides a reliable framework for hard-sphere reference systems. For the one-component hard-sphere fluid one remaining problem is the small deviation from computer simulation data of the structure at fluid densities close to freezing, as indicated in figure 1(b). For hard-sphere mixtures, high size asymmetries present the most challenging issue. Still one can consider the hard-core repulsion well taken care off by FMT. In my opinion, the most important future developments in classical equilibrium DFT will be the treatment of soft repulsions and attractions, additional to the hard-core repulsion at short distances, beyond simple perturbation theory approaches.

Acknowledgments

Almost from the first minute I started to work on DFT I had the pleasure to interact with and learn from Bob Evans. I want to acknowledge countless discussions and several collaborations with Bob from which I learned a lot about DFT in general and about FMT in particular. Bob also introduced me to Yasha Rosenfeld. My discussions with Yasha always left me impressed and inspired. I have also greatly benefited and enjoyed discussions and collaborations with Matthias Schmidt, Joe Brader, Paweł Bryk, Klaus Mecke, Gerhard Kahl, Peter König and Hendrik Hansen-Goos. Finally, I want to thank Ryo Akiyama, who invited me in November 2006 to give lectures on DFT in Fukuoka, Japan. The lecture notes I prepared for this occasion were a good starting point of this review.

References

[1] Evans R 1979 *Adv. Phys.* **28** 143
[2] Hohenberg P and Kohn W 1964 *Phys. Rev.* **136** B864
[3] Kohn W and Sham L J 1965 *Phys. Rev.* **140** A1133
[4] Mermin N D 1965 *Phys. Rev.* **137** A1441
[5] Rosenfeld Y 1989 *Phys. Rev. Lett.* **63** 980
[6] Vanderlick T K, Davis H T and Percus J K 1989 *J. Chem. Phys.* **91** 7136
[7] Percus J K 1976 *J. Stat. Phys.* **15** 505
[8] Reiss H, Frisch H L, Helfand E and Lebowitz J L 1960 *J. Chem. Phys.* **32** 119
[9] Percus J K and Yevick G J 1958 *Phys. Rev.* **110** 1
[10] Lebowitz J L 1964 *Phys. Rev.* **133** A895
[11] Rosenfeld Y 1988 *J. Chem. Phys.* **89** 4272
[12] Tarazona P and Evans R 1984 *Mol. Phys.* **52** 847
[13] Kierlik E and Rosinberg M L 1990 *Phys. Rev.* A **42** 3382
[14] Phan S, Kierlik E, Rosinberg M L, Bildstein B and Kahl G 1993 *Phys. Rev.* E **48** 618
[15] Rosenfeld Y, Schmidt M, Löwen H and Tarazona P 1996 *J. Phys.: Condens. Matter* **8** L577
[16] Rosenfeld Y, Schmidt M, Löwen H and Tarazona P 1997 *Phys. Rev.* E **55** 4245
[17] Tarazona P 2000 *Phys. Rev. Lett.* **84** 694
[18] Tarazona P 2002 *Physica* A **306** 243
[19] Roth R, Evans R, Lang A and Kahl G 2002 *J. Phys.: Condens. Matter* **14** 12063
[20] Lang A 2001 *Doctoral Thesis* Technical University of Vienna
[21] Hoover W G and Ree F H 1968 *J. Chem. Phys.* **49** 3609
[22] Noya E G, Vega C and de Miguel E 2008 *J. Chem. Phys.* **128** 154507
[23] Mansoori G A, Carnahan N F, Starling K E and Leland T W Jr 1971 *J. Chem. Phys.* **54** 1523
[24] Evans R 1992 *Fundamentals of Inhomogeneous Fluids* ed D Henderson (New York: Dekker) p 85
[25] Kihara T 1963 *Adv. Chem. Phys.* **5** 147
[26] Percus J K 1988 *J. Stat. Phys.* **52** 1157
[27] Kratky K W 1981 *J. Stat. Phys.* **25** 619
[28] Tutschka C and Kahl G 2000 *Phys. Rev.* E **62** 3640
[29] Roth R and Dietrich S 2000 *Phys. Rev.* E **62** 6926
[30] Kierlik E and Rosinberg M L 1991 *Phys. Rev.* A **44** 5025
[31] Tarazona P, Marconi U M B and Evans R 1987 *Mol. Phys.* **60** 573
[32] Rosenfeld Y 1993 *J. Chem. Phys.* **98** 8126
[33] Tarazona P and Rosenfeld Y 1997 *Phys. Rev.* E **55** R4873
[34] Tarazona P and Rosenfeld Y 1998 *New Approches to Problems in Liquid State Theory* ed C Caccamo, J P Hansen and G Stell (Doordrecht: Kluwer) p 293
[35] Schmidt M, Löwen H, Brader J M and Evans R 2000 *Phys. Rev. Lett.* **85** 1934
[36] Tarazona P, Cuesta J A and Martínez-Ratón Y 2008 *Lect. Notes Phys.* **753** 247
[37] Hansen-Goos H and Mecke K 2009 *Phys. Rev. Lett.* **102** 018302
[38] Rosenfeld Y 1994 *Phys. Rev.* E **50** R3318
[39] Rosenfeld Y 1995 *Mol. Phys.* **86** 637
[40] Gonzalez A, White J A, Roman F L and Velasco S 2006 *J. Chem. Phys.* **125** 064703
[41] Carnahan N F and Starling K E 1969 *J. Chem. Phys.* **51** 635

[42] Boublík T 1970 *J. Chem. Phys.* **53** 471
[43] Hansen J P and McDonald I R 1986 *Theory of Simple Liquids* (London: Academic)
[44] Yu Y-X and Wu J 2002 *J. Chem. Phys.* **117** 10156
[45] Hansen-Goos H and Roth R 2006 *J. Chem. Phys.* **124** 154506
[46] Hansen-Goos H and Roth R 2006 *J. Phys.: Condens. Matter* **18** 8413
[47] Bryk P, Roth R, Schoen M and Dietrich S 2003 *Europhys. Lett.* **63** 233
[48] Groot R D, Faber N M and van der Eerden J P 1987 *Mol. Phys.* **62** 861
[49] Noworyta J P, Henderson D, Sokołowski D and Chan K-Y 1998 *Mol. Phys.* **95** 415
[50] Cuesta J A, Martínez-Ratón Y and Tarazona P 2002 *J. Phys.: Condens. Matter* **14** 11965
[51] Dijkstra M, van Roij R and Evans R 1998 *Phys. Rev. Lett.* **81** 2268
[52] Dijkstra M, van Roij R and Evans R 1999 *Phys. Rev.* E **59** 5744
[53] Pagonabarraga I, Cates M E and Ackland G J 2000 *Phys. Rev. Lett.* **84** 911
[54] van Swol F and Henderson J R 1989 *Phys. Rev.* A **40** 2567
[55] Heni M and Löwen H 1999 *Phys. Rev.* E **60** 7057
[56] Henderson J R and van Swol F 1984 *Mol. Phys.* **51** 991
[57] Henderson J R 1983 *Mol. Phys.* **50** 741
[58] Henderson J R and Rowlinson J S 1984 *J. Phys. Chem.* **88** 6484
[59] Bryk P, Roth R, Mecke K R and Dietrich S 2003 *Phys. Rev.* E **68** 031602
[60] König P-M, Roth R and Mecke K R 2004 *Phys. Rev. Lett.* **93** 160601
[61] Roth R 2005 *J. Phys.: Condens. Matter* **17** S3463
[62] Tarazona P 1984 *Mol. Phys.* **52** 81
[63] Alder B J, Hoover W G and Young D A 1968 *J. Chem. Phys.* **49** 3688
[64] Young D A and Alder B J 1974 *J. Chem. Phys.* **60** 1254
[65] Groh B and Mulder B 2000 *Phys. Rev.* E **61** 3811
[66] Groh B 2000 *Phys. Rev.* E **61** 5218
[67] Ohnesorge R, Löwen H and Wagner H 1993 *Europhys. Lett.* **22** 245
[68] Lutsko J F 2006 *Phys. Rev.* E **74** 021121
[69] Warshavsky V B and Song X Y 2008 *J. Chem. Phys.* **129** 034506
[70] Rosenfeld Y 1990 *Phys. Rev.* A **42** 5978
[71] Cuesta J A 1996 *Phys. Rev. Lett.* **76** 3742
[72] Lafuente L and Cuesta J A 2002 *Phys. Rev. Lett.* **89** 145701
[73] Schmidt M 1999 *J. Phys.: Condens. Matter* **11** 10163
[74] Oosawa F and Asakura S 1954 *J. Chem. Phys.* **22** 1255
[75] Vrij A 1976 *Pure Appl. Chem.* **48** 471
[76] Schmidt M, Löwen H, Brader J M and Evans R 2002 *J. Phys.: Condens. Matter* **14** 9353
[77] Evans R, Brader J M, Roth R, Dijkstra M, Schmidt M and Löwen H 2001 *Phil. Trans. R. Soc.* A **359** 961
[78] Brader J M, Evans R, Schmidt M and Löwen H 2002 *J. Phys.: Condens. Matter* **14** L1
[79] Schmidt M 2000 *Phys. Rev.* E **63** 010101(R)
[80] Schmidt M 2004 *J. Phys.: Condens. Matter* **16** L351
[81] Roth R, Evans R and Dietrich S 2000 *Phys. Rev.* E **62** 5360
[82] Goulding D and Hansen J P 2001 *Mol. Phys.* **99** 865
[83] Goulding D and Melchionna S 2001 *Phys. Rev.* E **64** 011403
[84] Roth R and Evans R 2001 *Europhys. Lett.* **53** 271
[85] Oversteegen S M and Roth R 2005 *J. Chem. Phys.* **122** 214502
[86] Frink L J D and Salinger A G 2000 *J. Comput. Phys.* **159** 407
[87] Frink L J D and Salinger A G 2000 *J. Comput. Phys.* **159** 425
[88] Press W H, Teukolsky S A, Vetterling W T and Flannery B P 1996 *Numerical Recipes in C* (Cambridge: Cambridge University Press)